2002-05-13

# Singlet-Singlet and Triplet-Triplet Energy Transfer in Bichromophoric Cyclic Peptides

Mustafa Ozgur Guler
*Worcester Polytechnic Institute*

# Singlet-Singlet and Triplet-Triplet Energy Transfer in Bichromophoric Cyclic Peptides

By

Mustafa O. Guler

A Thesis submitted to the Faculty of the

Worcester Polytechnic Institute

In partial fulfillment of the requirements for the

Degree of Master of Science

In

Chemistry

By

_____

May 18, 2002

Approved:

_____

Dr. W. Grant McGimpsey, Major Advisor

_____

Dr. James P. Dittami, Department Head

## Abstract

Intramolecular singlet-singlet (SSET) and triplet-triplet (TTET) energy transfer have been studied in two cyclic octapeptides, 1A and 2A, and their open chain analogs, 1B and 2B. The peptides are constructed by a solid phase synthetic technique from enantiomerically pure amino acids with alternating chirality. Cyclic peptides with this arrangement of amino acids preferentially adopt flat, disk-like conformations where the peptide side chains lie on the outside of the ensemble. In 1A, benzophenone and naphthalene chromophores are incorporated as 4-benzoyl-L-phenylalanine and 2-naphtyl-L-alanine at positions 1 and 5 in the peptide sequence while in 2A, these chromophores occupy positions 1 and 3. Molecular modeling studies indicate that the interchromophore separation is larger in 1A than in 2A. This difference in separation is apparent from the observation of TTET energy transfer in 2A, which is consistent with the short range nature of TTET. Low temperature phosphorescence results indicate that intramolecular TTET is efficient in 2A and 2B and occurs with a rate of $k_{TTET} > 9.4x10^3\ s^{-1}$.

Intramolecular SSET occurs efficiently within these cyclic and open chain peptides. 1A undergoes intramolecular SSET from the

naphthalene chromophore to the benzophenone chromophore with $k_{SSET} > 3.7x10^7\ s^{-1}$, while in 2A with $k_{SSET} > 3.0x10^7\ s^{-1}$.

Results obtained by modeling, UV-Visible spectroscopy, fluorescence and phosphorescence spectroscopies and transient absorption experiments are described.

## Acknowledgements

I would like to thank my advisor Prof. W. Grant McGimpsey for his outstanding support and patience during this research. I appreciated the opportunity to work with him. The scientific fundamentals that I learned from him are going to build my future academic career.

I also would like to thank my friends and colleagues John Benco, Christopher Cooper, Dr Hubert Nienaber, Ernesto Soto, Veysel Yigit, Mine Ucak, Kathy Dennen, Cheryl Nowak, Nantanit Wanichechava and Selman Yavuz.

Finally I thank all chemistry and biochemistry faculty and graduate students for making this an enjoyable time.

## Table of Contents

## List of Figures

## List of Tables

## List of Schemes

## Introduction

Recently, there has been a remarkable increase in the number of literature papers about intramolecular charge and energy transfer in polychromophoric systems. Molecular electronic devices have been suggested as an application of transfer processes in such systems. Molecular wires[1], optoelectronic gates[2], switches[3] and rectifiers[4] are some of the devices envisioned and in each case device function is based on energy or electron transfer. (See Figure 1)

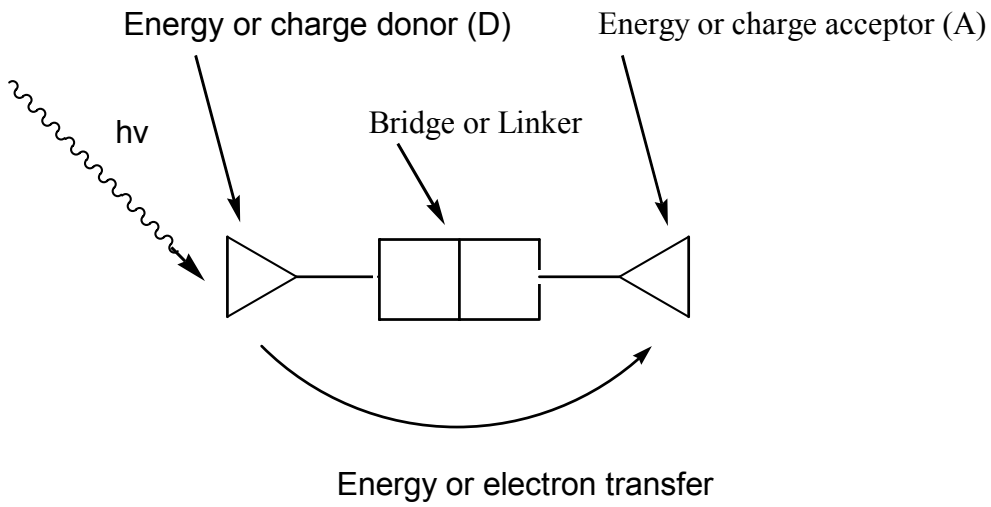


Figure 1: A molecular device.

Intramolecular energy transfer has been studied in various types of organic and organometallic systems[21] where the molecular architecture has been found to have a profound effect on the efficiency of the energy transfer. For example, flexibility of the spacer or linker between the energy donor and accepting groups (chromophores) has significant effects on the mechanisms and rates of energy transfer. Rigid saturated hydrocarbon bridges[5] promote efficient energy transfer via a through-bond mechanism. McGimpsey and co-workers have investigated intramolecular singlet-singlet energy transfer (SSET) and triplet-triplet energy transfer (TTET) in the rigid systems[5h] shown in Figure 2 and Figure 3 and found the dipole-induced dipole mechanism is sufficient to account for the SSET. Also Lindsey and Holten used rigidly-linked porphyrin units to study excited state energy migration and ground state electron hopping which were used for development of light harvesting antenna (Figure 4).[5m]

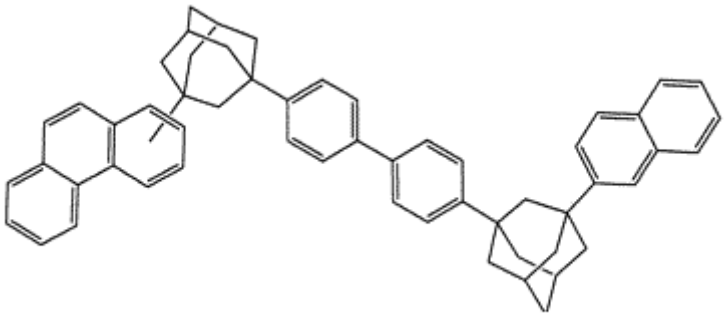

Figure 2: Rigid Adamantyl bridges between chromophores used by McGimpsey et al.

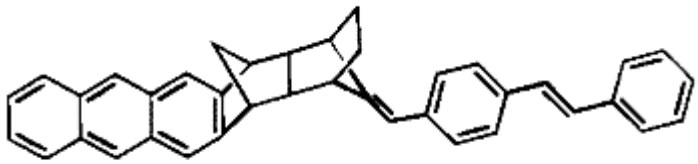

Figure 3: Rigid Norbornyl linkage used by McGimpsey et al.

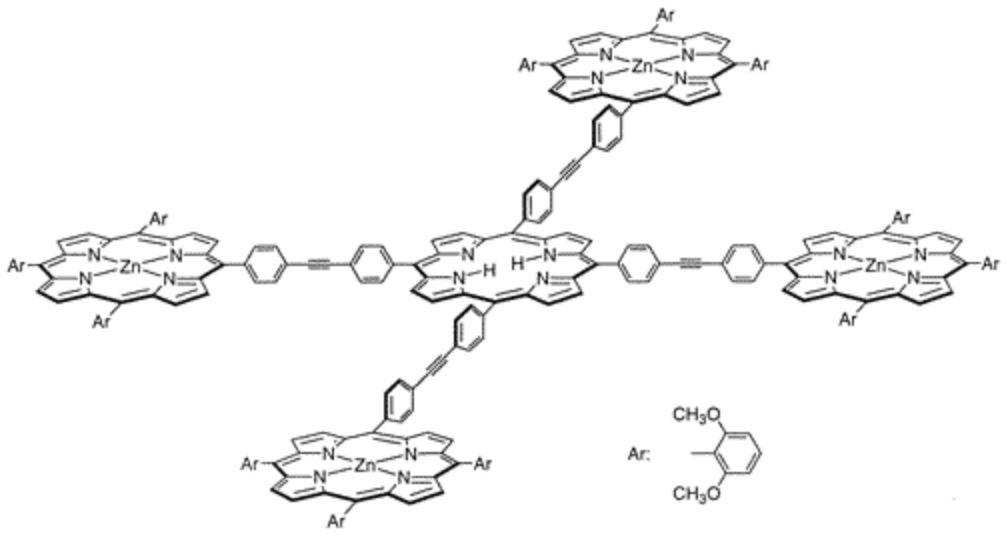


Figure 4: Light Harvesting Antenna used by Lindsey et al.

On the other hand, flexibly-linked donor and acceptor chromophores appear to undergo transfer via a through-space (through-solvent) process. For example methylene- and methyl ester- linked compounds and $\alpha$-helical peptides have been used as flexible spacers[6] (Figure 5)[5h]. In general, through-bond energy transfer is more rapid than through-space transfer.

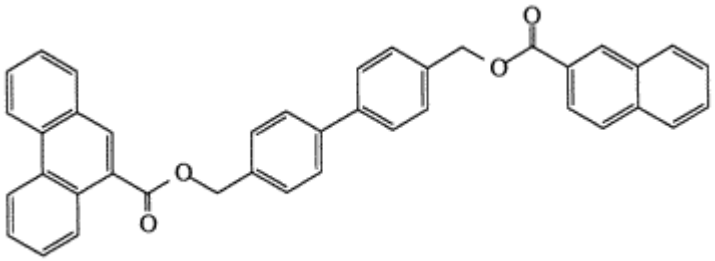


Figure 5: Methyl ester linkage used by McGimpsey et al.

In addition to linker rigidity and its effect on through-bond transfer efficiency, interchromophore separation is also a determining factor on the rate and mechanism of energy transfer. At small interchromophore distances, energy transfer can occur by both the exchange mechanism (Dexter)[7] and the dipole-induced dipole mechanism (Förster), while at larger interchromophore distances, only the dipole-induced dipole mechanism is operative.[8]

In addition to systems in which the chromophores are incorporated into the backbone of the molecule, intramolecular energy and charge transfer has also been studied in peptides containing chromophores that are appended to the peptide backbone (In effect the peptide serves as a non-interacting scaffold for the chromophore). Sisido and co-workers studied $\alpha$-helical bichromophoric polypeptides containing naphthalene and N,N-dimethylaniline.[9] They concluded that electron transfer between chromophores occurs by a through-space mechanism on the helical peptide. Fox and co-workers have studied intramolecular electron transfer with naphthalene and biphenyl chromophores which are separated by varying lengths of alanine oligopeptides.[10] They concluded that increasing the distance between the chromophores results in a decrease in the rate of transfer. Fox has also studied helical peptides to measure intramolecular charge

transfer in (N,N-dimethylaniline) / pyrene and (N,N-dimethylaniline) / naphthalene bichromophoric systems.[10a,10b] Transfer processes were thought to be through-space in molecules with larger chromophore separations and through-bond in peptides with smaller interchromophore distances. Our group has also studied intramolecular energy transfer between naphthalene and benzophenone chromophores in helical peptides.[11] McGimpsey and co-workers compared dipeptide and 14 residue helical peptides and found that the small interchromophore separations in the dipeptides studied result in efficient exchange transfer. However slower TTET was found for the helical peptide and was attributed to a larger interchromophore separation.

Given the importance of interchromophore separation on transfer rates and the desire to have high transfer rates in eventual devices, and also given the fact that in the systems studied to date, particularly the helical peptides, conformational flexibility results in a wide distribution of interchromophore separations, we have undertaken the study of energy transfer in a system that should possess sufficient conformational rigidity to limit the range of interchromophore separation and thereby make it possible to more accurately predict and optimize energy transfer rates. Thus, below we outline our study of energy transfer in cyclic D,L-$\alpha$ peptides.

Cyclic peptides have been suggested in possible sensors and drug delivery agents as well as catalysts and molecular electronic devices.[13] Ghadiri and coworkers characterized cyclic D, L -$\alpha$ peptides in 1993 by electron microscopy, electron diffraction, FT-IR and molecular modeling.[12] They concluded that cyclic peptides with an even number of alternating D and L amino acids can adopt low energy ring shaped flat conformations. In addition, amino acid side chains occupy equatorial positions along the cyclic peptide rings` edge. These conformational features leave backbone functionalities of each subunit unhindered and free to form hydrogen bonds with other rings leading to self-assembled cyclic peptide nanotubes (Figure 6).

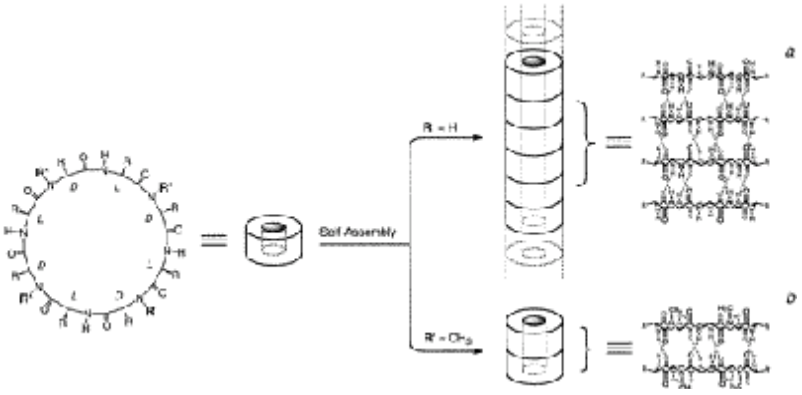

Figure 6: Cyclic peptide hydrogen bond formation

In this work our interest lies in the use of monomeric cyclic peptides functionalized with energy donor and acceptor chromophores. We have investigated the SSET and TTET processes in two cyclic peptides that each contain benzophenone and naphthalene chromophores, the archetypal energy transfer pair. We have designed the cyclic peptide so as to prevent supramolecular stacking into nanotubes by incorporating α-aminoisobutyric acid residues in the peptide backbone. Ghadiri et al. [14] have shown previously that the steric bulkiness of these residues disrupts H-bonding and prevents stacking.

In addition to the cyclic peptide we have also investigated their open-chain analogs. Model compounds in this study were the individual amino acids, i.e., alanine residues containing either benzophenone or naphthyl chromophores.

In order to discuss energy transfer in cyclic peptides, it is necessary to review the synthetic aspects of peptide preparation as well as the mechanisms of energy transfer.

**Solid phase Peptide Synthesis**

The peptides have been constructed by a solid phase synthetic technique from enantiomerically pure amino acids with alternating chirality. Construction of peptides on an insoluble solid support has obvious benefits, including the ease of the separation of peptide from soluble reagents, removal of excess reagents used for coupling, minimizing material losses and maximizing yields.

Solid phase peptide synthesis was first proposed by R.B. Merrifield in 1962 and his first paper was published in 1963.[18] Merrifield described the preparation of a tetrapeptide by successive addition of benzyloxycarbonylaminoacids to a polystyrene resin. He also made successive syntheses with *t*-butoxycarbonyl-protected aminoacids.[19] The Merrifield solid phase peptide synthesis technique has made peptide synthesis economical, simple and rapid. Subsequently different types of solvents, reagents and protecting groups have been used to make the synthesis more efficient. This included the use of the 9-fluorenylmethoxycarbonyl (Fmoc) on N-terminus protecting group[20], a method we have used in this work and which we describe below.

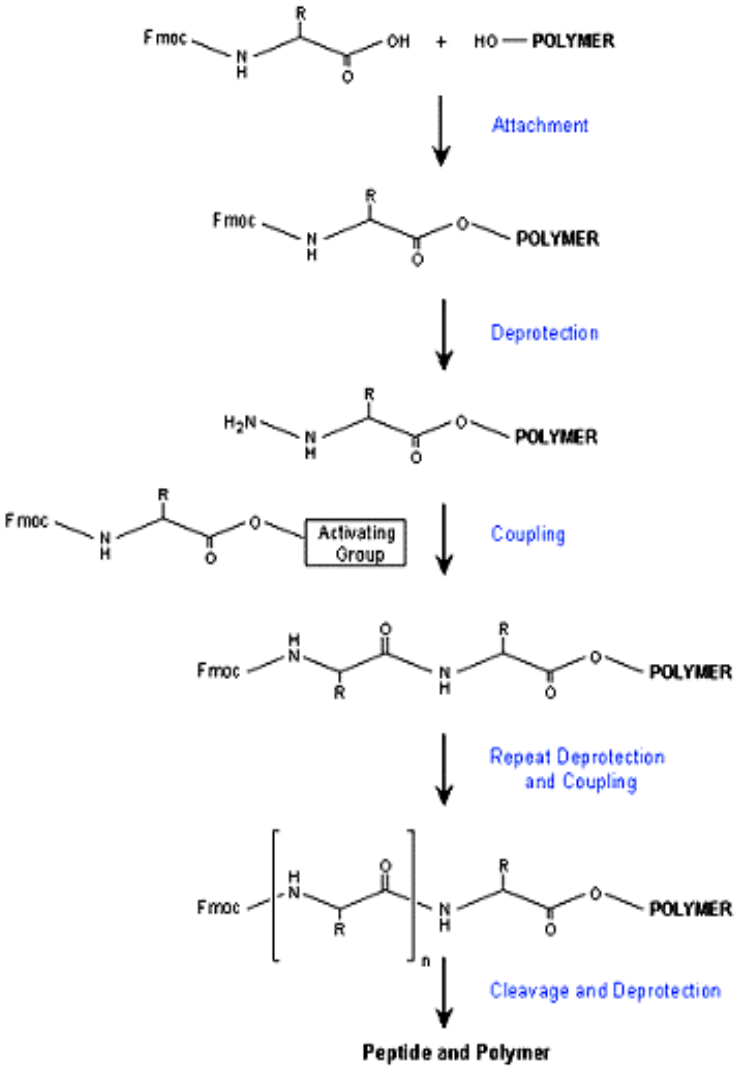


**General Scheme for Fmoc Synthesis**

Figure 7: Fmoc Strategy reaction table

Initially, the first Fmoc amino acid is attached to an insoluble support resin via an acid labile linker (Figure 7). Deprotection of the Fmoc protecting group, is accomplished by treatment of the resin

with a base, typically piperidine (Scheme 1). The second Fmoc protected amino acid is coupled utilizing a preactivated species or *in situ* activation (Scheme 2). After coupling, excess reagents are removed by washing the resin. This process is repeated until the desired peptide sequence is assembled. In the final step, the resin-bound peptide is deprotected and then detached from the solid support via TFA cleavage.

The mechanism for the deprotection of the protecting group is shown in scheme 1.

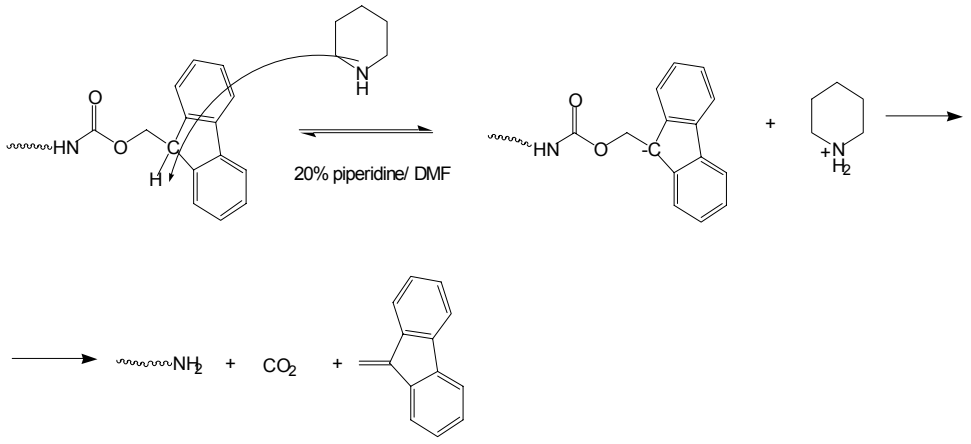


Scheme 1

The mechanism of the activation of protected amino acids for coupling reaction is shown in scheme 2.

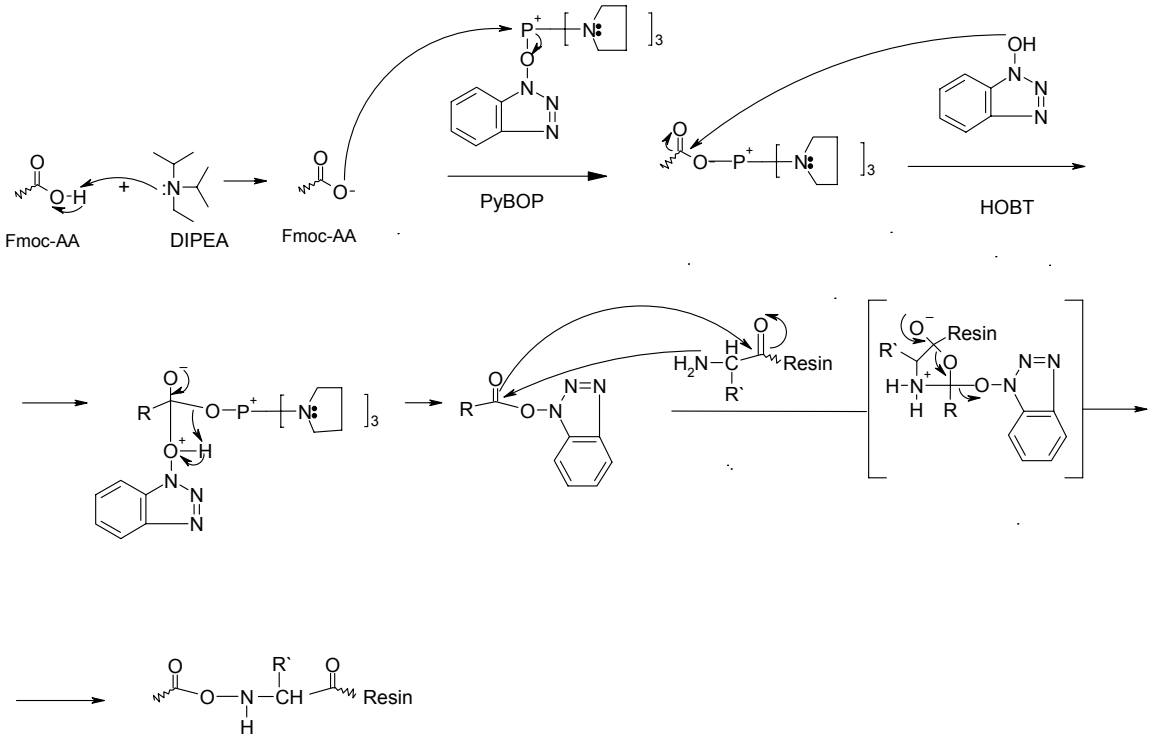


Scheme 2

## Energy Transfer Mechanisms

### The Coulombic Interaction (Förster Mechanism)

The Coulombic mechanism (dipole-induced dipole or Förster) involves the induction of a dipole oscillation in the acceptor A by the excited donor, D*. Oscillation of the excited state donor dipole induces oscillations in the acceptor`s dipole. In energy transfer, energy lost by the donor molecule is gained by the acceptor. Excitation is transferred through space, and can be likened to a radio transmitter acting on a radio receiver. This type of energy transfer does not require orbital overlap or collision between the donor and acceptor molecule. Therefore energy transfer by this mechanism can occur over large molecular scale interchromophore separations (> 100 Å). Förster showed the distance dependence of the dipole-induced dipole mechanism by equation 1, where $k_{ET}$ is the rate of energy transfer, $k_D$ is the decay rate for the donor excited state, R is the interchromophore separation and $R_0$ is the Förster critical distance for energy transfer which is the distance at which 50% of the excited state decays by energy transfer.

$$k_{ET} = k_D ( R_0/R )^6 \qquad \textbf{(1)}$$

$R_0$ is calculated by overlap of the emission spectrum of D* and the absorption spectrum of A (equation 2).

$$R_0^6 = \frac{9100(\ln 10)\Phi_D \kappa^2}{128\eta^4 \pi^5 \mathrm{N}_A} J \qquad \textbf{(2)} \qquad J = \frac{\int_0^\infty f_D(\nu)\varepsilon_A(\nu)\nu^{-4} d\nu}{\int_0^\infty f_D(\nu)}$$

Here, $\Phi_D$ is the fluorescence quantum yield of the donor in the absence of acceptor, η is the refractive index of the solvent, $N_A$ is the Avogadro's number, $\kappa^2$ is a term that describes the relative orientation of the transition dipoles for the donor and acceptor groups and in the case of freely rotating chromophores is usually assigned a value of 2/3. R is the distance between donor and acceptor, $R_0$ is the critical Förster transfer distance and *J* is the spectral overlap integral of donor and acceptor.[17]

Since TTET involve the conversion of a singlet ground state acceptor to an excited triplet state and since the oscillator strength of $S_0$ to T transitions is usually very small, the spectral overlap integration is small for TTET, leading to a small value of $R_0$ calculated from equation 1 and a small $k_{ET}$. On the other hand SSET can have large Förster rate constants.

**The Exchange Interaction**

The exchange interaction or Dexter mechanism can be visualized as electron tunneling where one electron moves from the excited donor lowest unoccupied molecular orbital to the acceptor lowest unoccupied molecular orbital while an electron moves from the acceptor highest occupied molecular orbital to the donor highest occupied molecular orbital. Therefore in exchange energy transfer, the exchange resonance interaction of D* and A occurs via overlap of electron clouds and requires collision between the molecules.

The distance dependence of this mechanism is expressed by Dexter as;

$k_{ET}$ (exchange) = K J exp ($-2R_{DA}/L$) **(3)**

where K is related to the specific orbital interactions, J is a spectral overlap integral normalized to the extinction coefficient of the acceptor, $R_{DA}$ is the donor and acceptor separation and L is the van der Waals radii.

TTET and SSET can occur efficiently by this mechanism as long as there is collision between the donor and the acceptor molecule. The efficiency of the energy transfer through this mechanism drops off

exponentially whereas in the dipole-induced dipole mechanism it is related to the inverse sixth power of intercromophore separation.

## Experimental Section

### General Methods

$^{1}$Proton nuclear magnetic resonance ($^{1}$H NMR) spectra were obtained on a Bruker AVANCE 400 (400 MHz) NMR spectrometer. Chemical shifts are reported in ppm ($\delta$) relative to internal tetramethylsilane (TMS) at 0.00 ppm. $^{13}$Carbon nuclear magnetic resonance ($^{13}$C NMR) spectra were recorded with the same spectrometer mentioned above. FTIR spectra were obtained on a Nexus 670 FT-IR ESP instrument equipped with a Nicolet Smart Golden Diamond ATR system. Reverse-phase high performance liquid chromatography (RP-HPLC) was used for identification and purification of the peptides (mobile phase: acetonitrile/0.1% TFA in water. A semi-Preparative Zorbax Rx-C18 column (9.4x250 mm, 80 Å, 5 µm particle size) and an analytical Zorbax Rx-C18 column (4.6x250 mm, 80 Å, 5 µm particle size) were used for these analyses. Mass spectra (electrospray) were performed by SYNPEP Corporation, Dublin, CA. Analytical thin layer chromatography was performed using precoated Whatman 250 µm K5F silica gel 150 Å normal phase plates with visualization by UVlamp or in a glass chamber containing iodine. Preparative thin layer chromatography

was performed using 1000 μm precoated Whatman PK6F 60 Å silica gel plates.

**Materials**

Unless otherwise noted, all reagents and solvents for spectroscopic and laser studies were used as received from Aldrich and were spectrophotometric grade. Acetonitrile for HPLC was Aldrich HPLC grade. Fmoc-3-(2-naphthyl)-L-alanine, t-Boc-3-(2-naphthyl)-L-alanine, Fmoc-(4-benzoyl)-L-phenylalanine and t-Boc-(4-benzoyl)-L-phenylalanine were used as received from AdvancedChemTech. Coupling reagents and other amino acids were purchased from NovaBioChem. Diisopropylethylamine (DIPEA) was purchased from VWR Scientific products (99%). All other chemical reagents for synthesis were from Aldrich.

**Synthesis of Peptides**

Peptide synthesis was performed by the stepwise elongation of N-Fmoc amino acids on a preloaded N-Fmoc-L-Ala Wang resin. The resin was swelled for 45 min before the first deprotection. Coupling

was performed in 10 ml DMF per 1 g of resin. Amino acids were deprotected using 20% piperidine in DMF for 9 min and couplings were performed using 2.5 eq amino acids, 2.5 eq HOBT, 2.5 eq PyBOP, 5 eq DIPEA in DMF. Washing with DMF (3 times at 20 ml), MeOH (3 times at 20 ml), EtOH (3 times at 20 ml) and DMF (3 times at 20 ml) was done between each coupling and deprotection. Double couplings were performed in DMF for 8 h for each amino acid coupling. After the final deprotection and regular washings, the resin was washed with MeOH (3 times at 20 ml), EtOH (3 times at 20 ml) DCM (3 times at 20 ml) and dried *in vacuo*. Deprotected peptide was cleaved from the resin by treatment with 97.5% TFA and 2.5% water (v/v) for 4 h. The crude mixture was filtered and concentrated to 2 ml under reduced pressure. The peptide was then precipitated by the addition of cold diethyl ether and subsequently dried *in vacuo* overnight.

**Ala-Aib-Bpa-Aib-Ala-Aib-Npa-Aib** (**1B**). The open chain octapeptide was purified by RP-HPLC. **1B** was identified by its absorbance at 224 nm in 50% (0.1% TFA/water) / 50% Acetonitrile mobile phase at a flow rate 2.5 ml/min. $^{1}$H NMR (400 MHz, 293 K, $CD_3OD$): Ala and Aib, $CH_3$ (m 1.2-1.5); Ala, Bpa and Npa, CH (m 3.0-3.6); Bpa and Npa, $CH_2$ (m 4.0-4.8); N-H, N-$H_2$, Bpa and Npa,

aromatic CH (m 7.2-8.2). $^{13}C$ NMR ($CD_3OD$): Ala, Bpa and Npa, CH (50.0, 53.2, 56.5, 57.1); Npa and Bpa, $CH_2$ (37.7, 38.3); Aib and Ala, $CH_3$ (16.9-27.7); Bpa and Npa, aromatic C (127.2-134.2). ESI-MS: M calculated = 949.1, M found = 949.6. IR: amide I, 1658 $cm^{-1}$ ; amide II, 1529 $cm^{-1}$ ; N-H stretch 3300 $cm^{-1}$.

**Ala-Aib-Bpa-Aib-Npa-Aib-Ala-Aib** (**2B**). The open chain octapeptide was identified by RP-HPLC with its absorbance at 224 nm in 25% (0.1% TFA/water) / 75% Acetonitrile mobile phase at a flow rate 3 ml/min. $^1H$ NMR (400 MHz, 293 K, $CD_3OD$): Ala and Aib, $CH_3$ (m 1.1-1.8); Ala, Bpa and Npa, CH (m 3.0-3.7); Bpa and Npa, $CH_2$ (m 4.1-4.8); N-H, N-$H_2$, Bpa and Npa, aromatic CH (m 7.0-8.5). $^{13}C$ NMR ($CD_3OD$): Ala, Bpa and Npa, CH (49.5, 50.0, 57.0, 57.7); Npa and Bpa, $CH_2$ (37.5, 38.0); Aib and Ala, $CH_3$ (17.4-27.7); Bpa and Npa, aromatic C (117.0-134.3). ESI-MS: $MH^+$ calculated = 950.1, $MH^+$ found = 950.5. IR: amide I, 1658 $cm^{-1}$ ; amide II, 1529 $cm^{-1}$ ; N-H stretch 3300 $cm^{-1}$.

**Octapeptide Cyclization**

The open chain octapeptide, 10 eq DIPEA, 1.3 eq HOAT, 1.3 eq HATU were dissolved in DMF in a round bottom flask. The mixture

was stirred at 0 $^{0}$C for 3 h in an ice bath. DMF was removed *in vacuo*. The resulting cyclized peptide was precipitated and washed using cold diethyl ether.

**Cyclo(Ala-Aib-Bpa-Aib-Ala-Aib-Npa-Aib)** (**1A**). Cyclic octapeptide was detected at $R_F$ 0.4 on analytical TLC plate in 1:2:20 AcOH:MeOH:DCM solution. Prep TLC was used for purification of **1A**. Also **1A** was identified by RP-HPLC with its absorbance at 224 nm in 60% (0.1% TFA/water) / 40% Acetonitrile mobile phase at a flow rate 2.5 ml/min. $^{1}$H NMR (400 MHz, 293 K, $CD_3OD$): Ala and Aib, $CH_3$ (m 1.0-1.6); Ala, Bpa and Npa, CH (m 3.0-3.5); Bpa and Npa, $CH_2$ (m 4.0-4.5); N-H, Bpa and Npa, aromatic CH (m 7.0-8.0). $^{13}$C NMR ($CD_3OD$): Ala, Bpa and Npa, CH (51.6, 57.2, 57.6); Npa and Bpa, $CH_2$ (37.0, 37.3); Aib, $CH_3$ (24.4, 25.3, 27.8, 31.3); Ala, $CH_3$ (18.9); Bpa and Npa, aromatic C (126.5-134.2). ESI-MS: $M+Na^+$ found= 953, $M+Na^+$= calculated 954. IR: amide I, 1658 cm$^{-1}$ ; amide II, 1538 cm$^{-1}$ ; N-H stretch 3308 cm$^{-1}$.

**Cyclo(Ala-Aib-Bpa-Aib-Npa-Aib-Ala-Aib)** (**2A**). The cyclic octapeptide was purified by recrystallization from acetonitrile and diethyl ether. It was also identified by RP-HPLC with its absorbance at 224 nm in 30% (0.1% TFA/water) / 70% Acetonitrile mobile

phase at a flow rate 2 ml/min. $^{1}H$ NMR (400 MHz, 293 K, $CD_3OD$): Ala and Aib, $CH_3$ (m 1.0-2.0); Ala, Bpa and Npa, CH (m 3.0-3.5); Bpa and Npa, $CH_2$ (m 4.0-4.6); N-H, Bpa and Npa, aromatic CH (m 7.0-8.7). $^{13}C$ NMR ($CD_3OD$): Ala, Bpa and Npa, CH (55.8, 56.2, 56.5, 57.5); Npa and Bpa, $CH_2$ (38.2, 38.7); Aib and Ala, $CH_3$ (24.4-26.4); Bpa and Npa, aromatic C (127.0-134.3). ESI-MS: $M+Na^+$ found= 953.5, $M+Na^+$ calculated= 954. IR: amide I, 1658 $cm^{-1}$ ; amide II, 1538 $cm^{-1}$ ; N-H stretch 3310 $cm^{-1}$.

**Molecular Modeling Calculations**

Molecular modeling was performed on an SGI 320 running Windows NT. Calculations were carried out using the Molecular Operating Environment (MOE) ver. 2000.02 computing package (Chemical Computing Group Inc., Montreal, Quebec, Canada.). Structures were minimized first using the AMBER94 potential control under a solvent dielectric of 38. PEF95SAC was used to calculate partial charges. Molecular structures were then subjected to a 30 ps molecular dynamics simulation employing the NVT statistical ensemble. The structures were heated to 400 K, equilibrated at 290 K and cooled down to 280 K in the dynamics thermal cycle at a rate of 10 K/ps.

The charge densities were also probed computationally using ChemPlus 1.5 and the MM+ force field. The lowest energy conformations were further minimzed using AM1 and PM3 parameters in the Hyperchem semi-empirical option. These minimized conformations were used to obtain the spectroscopic energies with ZINDO/S parameters.

## Spectroscopic Methods

### UV-Visible Spectroscopy

Ground state absorption spectra and extinction coefficients were obtained with a Shimadzu 2100U absorption spectrometer with samples contained in 1 cm x 1 cm quartz cuvettes. Samples were measured in single beam mode compared with a blank obtained with pure solvent. Extinction coefficients for each wavelength were calculated by Beer`s law from the average of three different samples having different concentrations.

### Emission Spectroscopy

Fluorescence emission spectra were measured in nitrogen-saturated acetonitrile in 1 cm x 1 cm quartz cuvettes using a Perkin Elmer LS-50B specrofluorimeter. Samples were prepared with an O.D. < 0.05 at the excitation wavelength. Phosphorescence spectra were recorded at 77 K with the same instrument. Samples were contained in a 2 mm I.D. quartz tube and were dissolved in 1:1 methanol:ethanol glasses.

**Laser Flash Photolysis**

Nitrogen saturated samples were prepared with O.D. = 0.3-0.5 at the excitation wavelength. Samples were run in a specially constructed 7 mm x 7 mm quartz flow cell with a peristaltic pump. Samples were irradiated with the pulses of Continuum Nd:YAG laser using the quadrupled wavelength of 266 nm.

**Apparatus**

In general, the system includes a sample cell, laser, monitoring source, optical train, detector, and a data I/O system (digitizer/computer).

**Sample Cell**

Sample cells were 3 mL quartz tubes (7 mm x 7 mm). Solutions were prepared at concentrations to yield absorbances in the range of 0.3-0.5 at the excitation wavelength. Samples were out-gassed for at least 10 min with nitrogen. Always specially constructed flow cell was used.

For the flow system, 100 ml samples were prepared and placed into a 125 ml reservoir for at least 45 min of out-gassing with nitrogen. The sample was caused to flow through the quartz cell via an Easy-load MasterFlex Model 7518-00 peristaltic pump. The flow

rate was adjusted such that a fresh volume of sample was exposed to each laser pulse.

**Laser system**

The laser source was a Continuum Nd-YAG laser with fourth harmonic generation (266 nm) operating at 8 mJ/pulse and 5 ns/pulse.

**Monitoring source**

The monitoring lamp was a 150 W ORIEL Xenon Arc lamp generating a continuum from 200 to the IR and operated in pulsed mode. A lamp pulser triggers the lamp power supply which increases the current from 6 to 30 amps for a duration of 4 ns. This monitoring beam is focused, along the optical train into the sample cell holder, through a 2 mm pinhole.

**Optical train**

Shutters were used along the excitation and monitoring pathways to protect the sample from unnecessary photolysis. Lenses were used to concentrate the excitation source and monitoring source into the sample holder as well as the transmission of the monitoring light to the monochromator. Cutoff filters were employed to eliminate second order effects.

**Detector**

The detector was a 27.5 cm focal length monochromator from Acton Research Corp. It employed a wavelength-neutral holographic grating with 1200 groves/mm or a conventional grating blazed at 750 mm with 1200 groves/mm. A Burle 4840 photomultiplier tube was located at the monochromator exit slit. It was wired in a six-dynode chain for fast response and to prevent saturation at high intensities. The electrical current amplification was controlled by adjustment of a voltage applied to the central dynode and was kept within the linear working range of the photomultiplier.

**Data I/O system**

A Tektronix 7912HB transient digitizer with a Tekronix 7A29P vertical amplifier plug-in and a Tekronix 7B90P horizontal plug-in was used to convert the photomultiplier output to digital form and transfer it to the processing computer.

Raw data is obtained in the form of monitoring beam intensity ($I_0$), in volts, as a function of time. This is converted to $I_t$, intensity transmitted through the sample, and then to optical density (O.D.), equation 4.

$$O.D. = \log(I_0/I_t) \qquad \textbf{(4)}$$

Since $I_t$ may be representative of transient production as well as ground state depletion, O.D. is expressed as $\Delta$O.D., equation 5.

$$\Delta O.D. = \log[(I_0 - I_\infty)/(I_t - I_\infty)] \qquad \textbf{(5)}$$

To interface between the computer and the rest of the system, a Sciemetric Labmate Intelligent Lab Interface was used. The triggering of the monitoring lamp pulser, baseline compensator, digitizer and lasers was controlled by a DG535 Stanford Research Systems digital delay pulse generator.

A typical experimental sequence is as follows. Initially, both the laser shutter and the monitoring lamp shutter are opened allowing the monitoring lamp light to pass through. The lamp pulser then fires the lamp power supply transmitting the light through the sample cell to the monochromator and the photomultiplier (PM) producing an electrical signal. This signal is transferred to the backoff unit that stores the $I_0$ value. The digitizer is then triggered to start data collection from the PM, (time scale for data collection ranged from 5 to 50 $\mu$s). The laser is then fired to produce transient species within the sample cell thereby changing the intensity of

monitoring light. The data is then transferred to the computer for analysis.

For each sampling, 5 - 10 laser pulses are averaged together to increase the signal-to-noise ratio. Additionally, a fluorescence correction is also used to compensate for laser induced fluorescence. This is accomplished by firing the laser with no lamp output and subtracting the resulting trace from the data profile.

Kinetic decay or growth data is analyzed for first or second order behavior at the individual wavelengths of the observed transients.

Absorption spectra are obtained as $\Delta$O.D. values vs. wavelength as a function of time after the laser pulse.

## Summary of Compounds

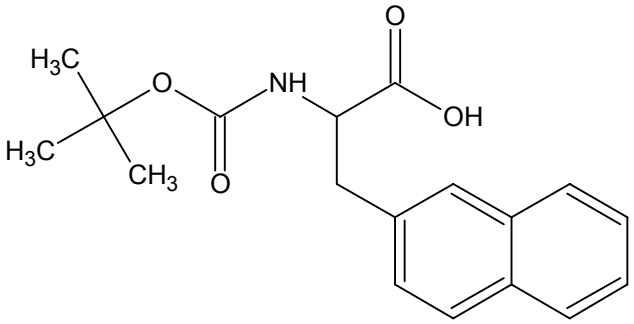


**Boc-2-Nal-OH**

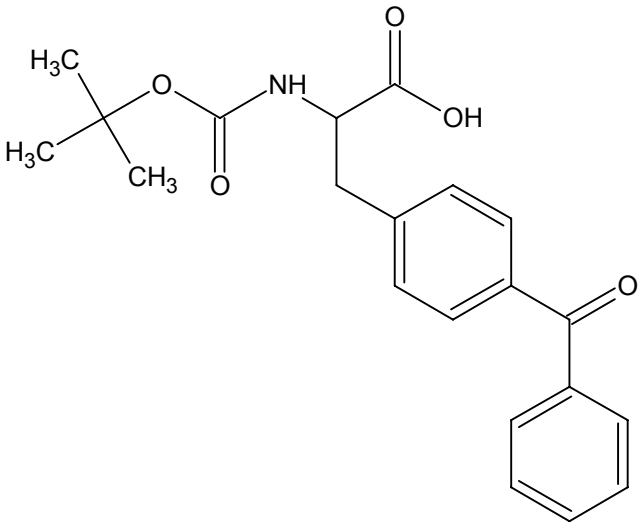


**Boc-Bpa-OH**

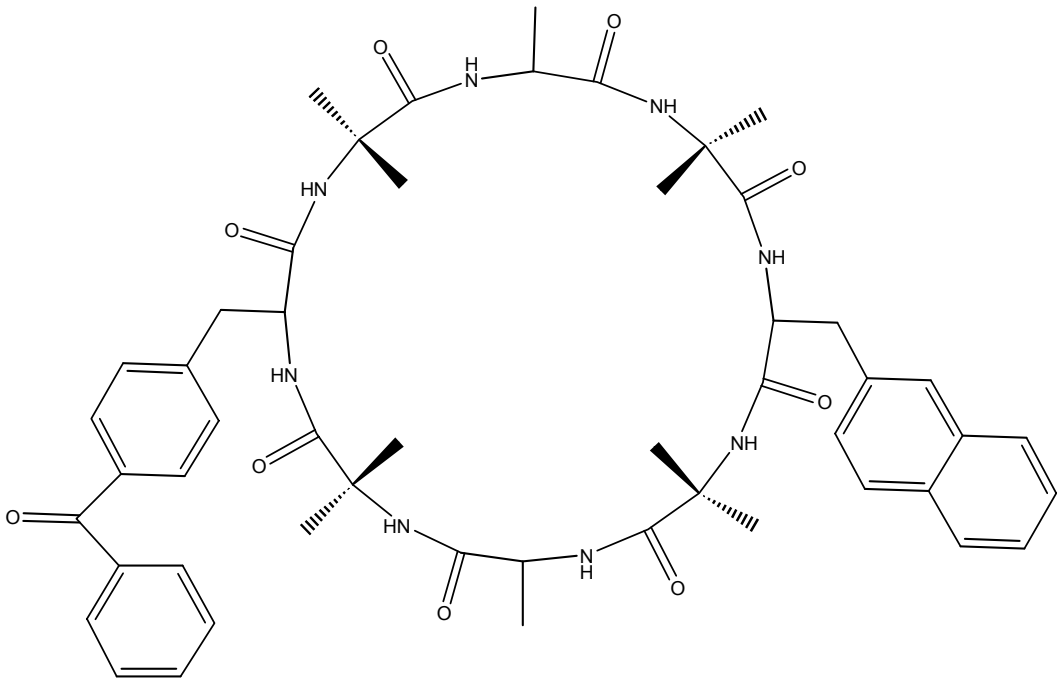

**1A**

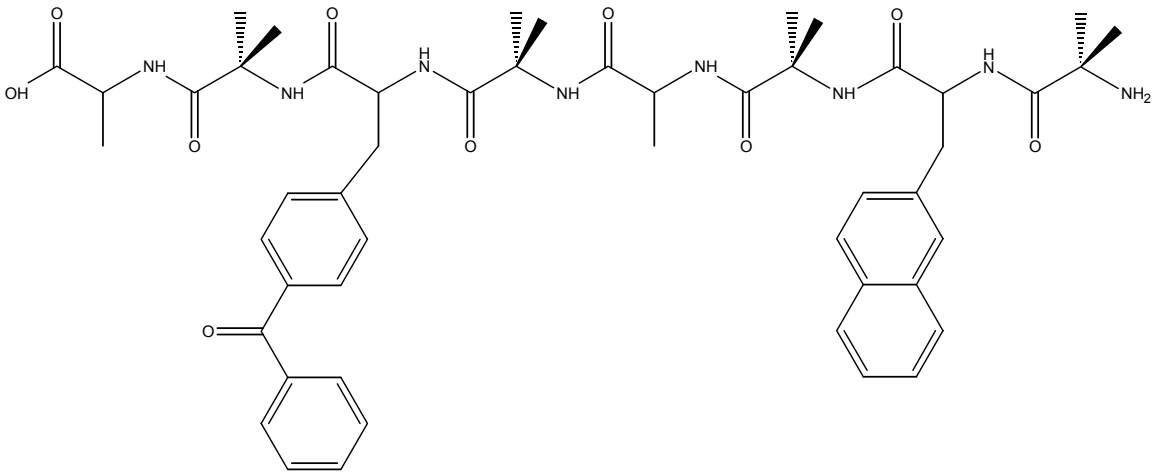

**1B**

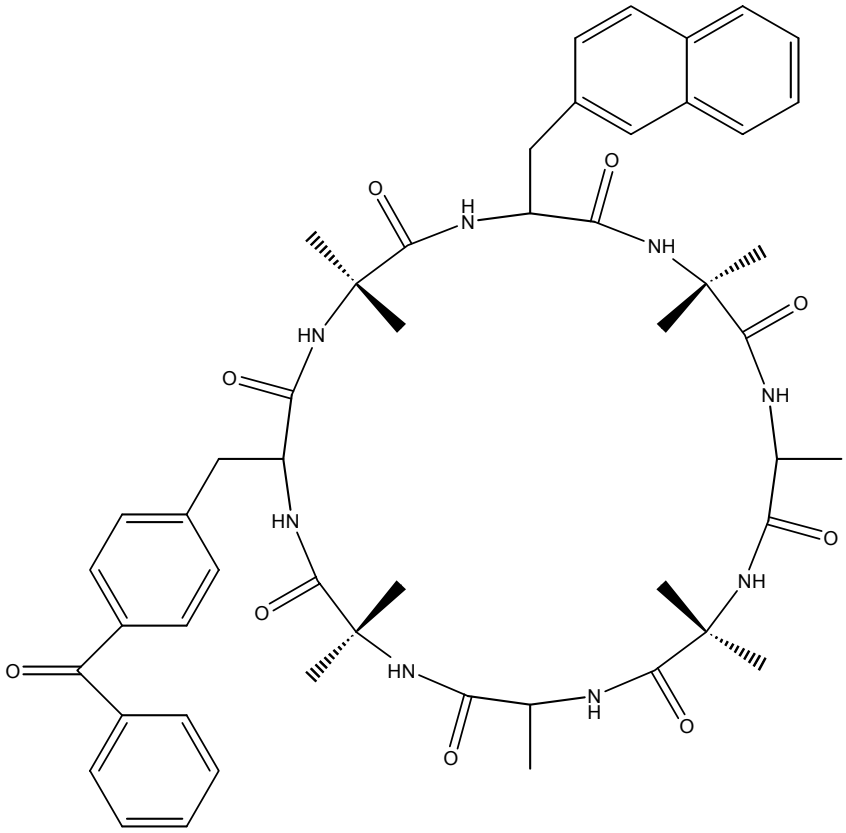


**2A**

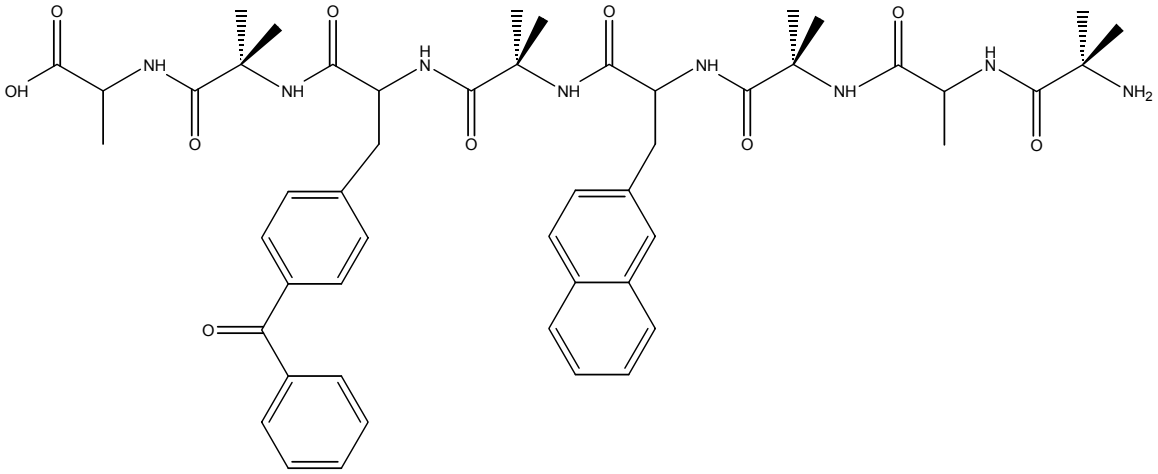

**2B**

## Results

Spectroscopic results for compound Boc-2-Nal-OH, Boc-Bpa-OH, 1A and 1B are shown in Figures 8-16.

Figure 8: Extinction coefficient plot for Boc-2-Nal-OH

Figure 9: Extinction coefficient plot for Boc-Bpa-OH

Figure 10: Extinction coefficient plot for 1A

Figure 11: Extinction coefficient plot for 1B

Figure 12: Fluorescence spectra of Boc-2Nal-OH, 1A and 1B at an excitation wavelength of 224 nm

Figure 13: Fluorescence spectra of Boc-2Nal-OH, 1A and 1B at an excitation wavelength of 266 nm

Figure 14: Fluorescence spectra of Boc-2Nal-OH, 1A and 1B at an excitation wavelength of 280 nm

Figure 15: Phosphorescence spectra of Boc-Bpa-OH, 1A and 1B at an excitation wavelength of 266 nm

Figure 16: Transient absorption spectra of Boc-2Nal-OH, Boc-Bpa-OH, 1A and 1B at an excitation wavelength of 266 nm

**Figure 8: Extinction coefficient plot for Boc-2-Nal-OH**

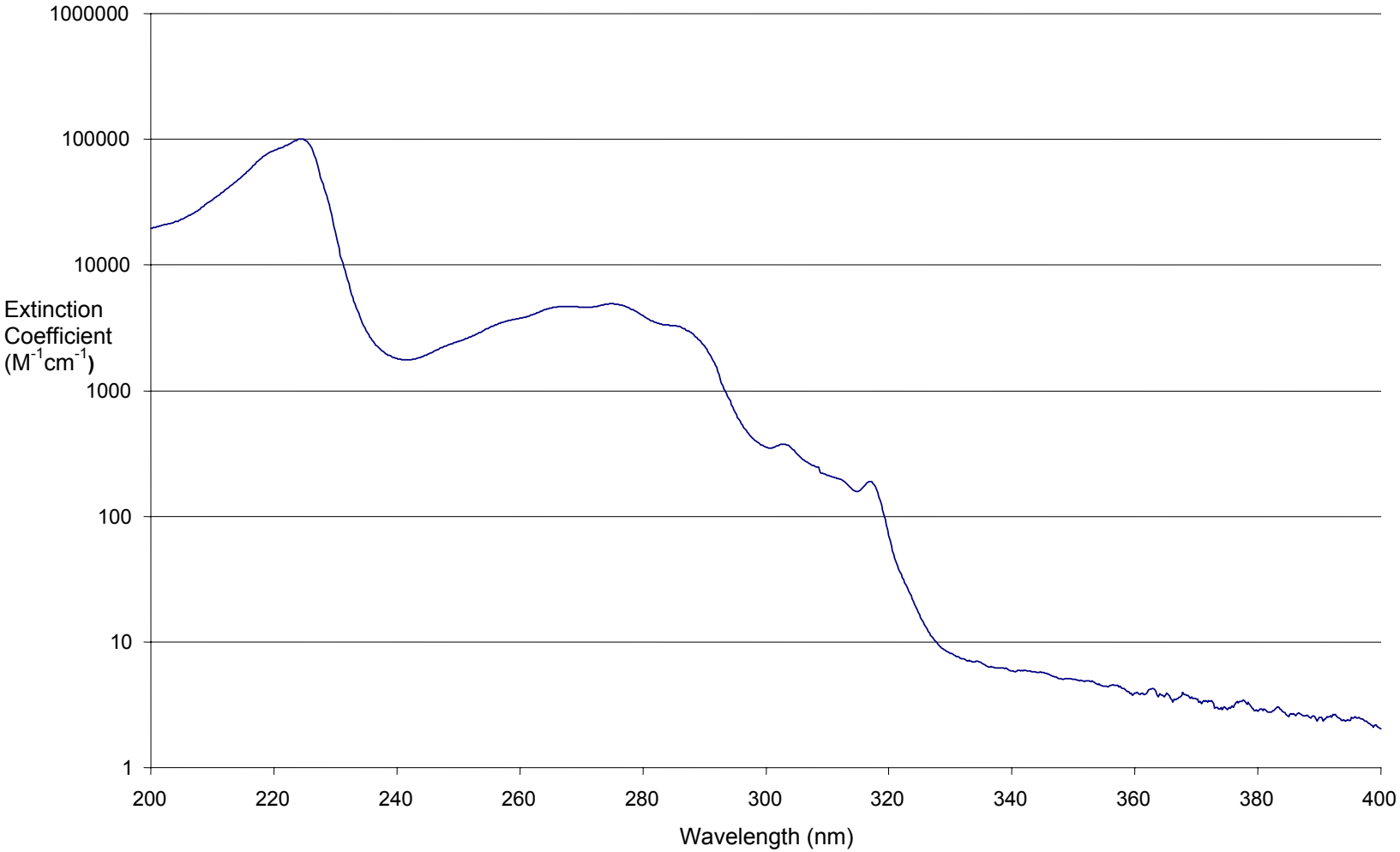

**Figure 9: Extinction coefficient plot for Boc-Bpa-OH**

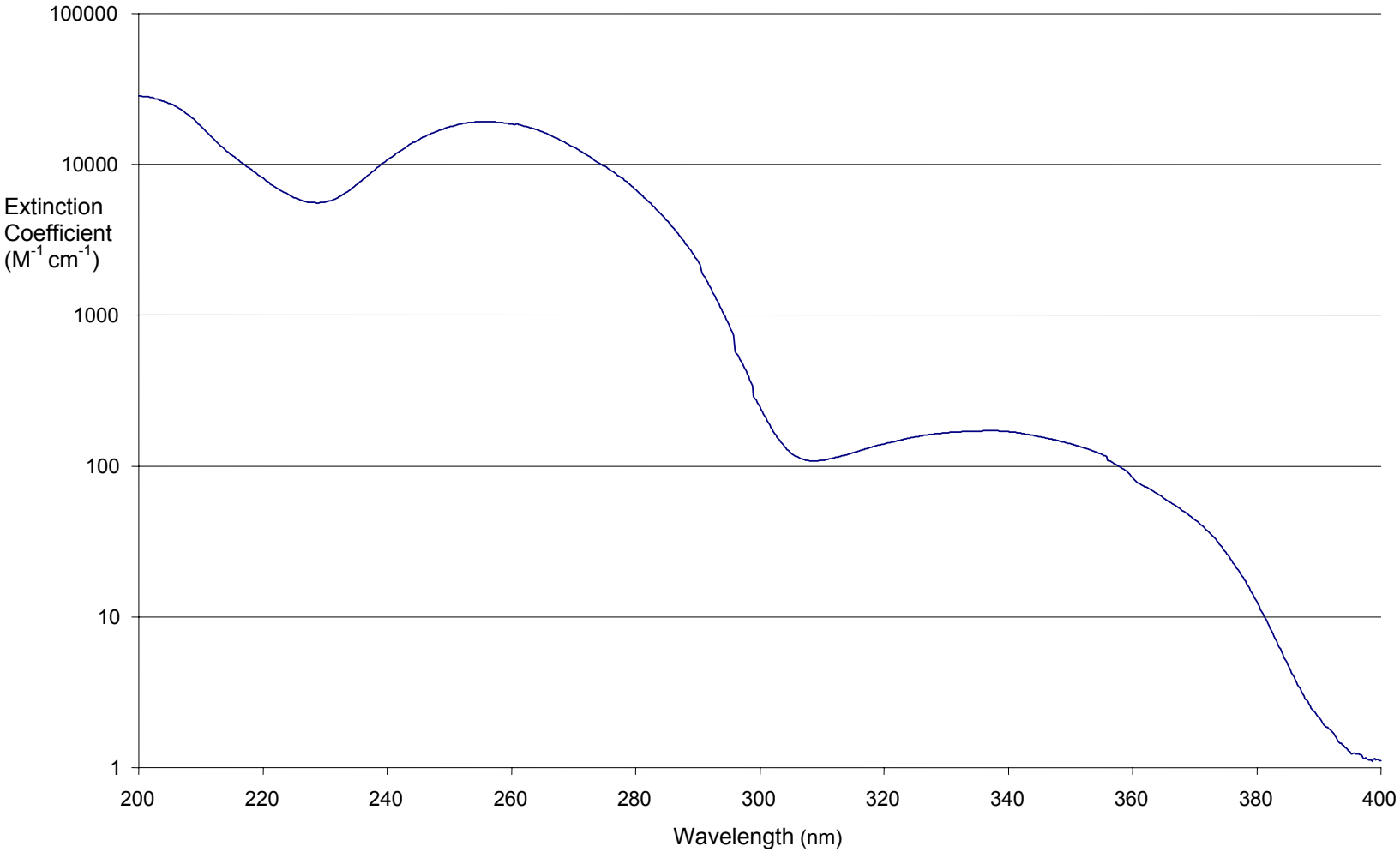

**Figure 10: Extinction coefficient plot for 1A**

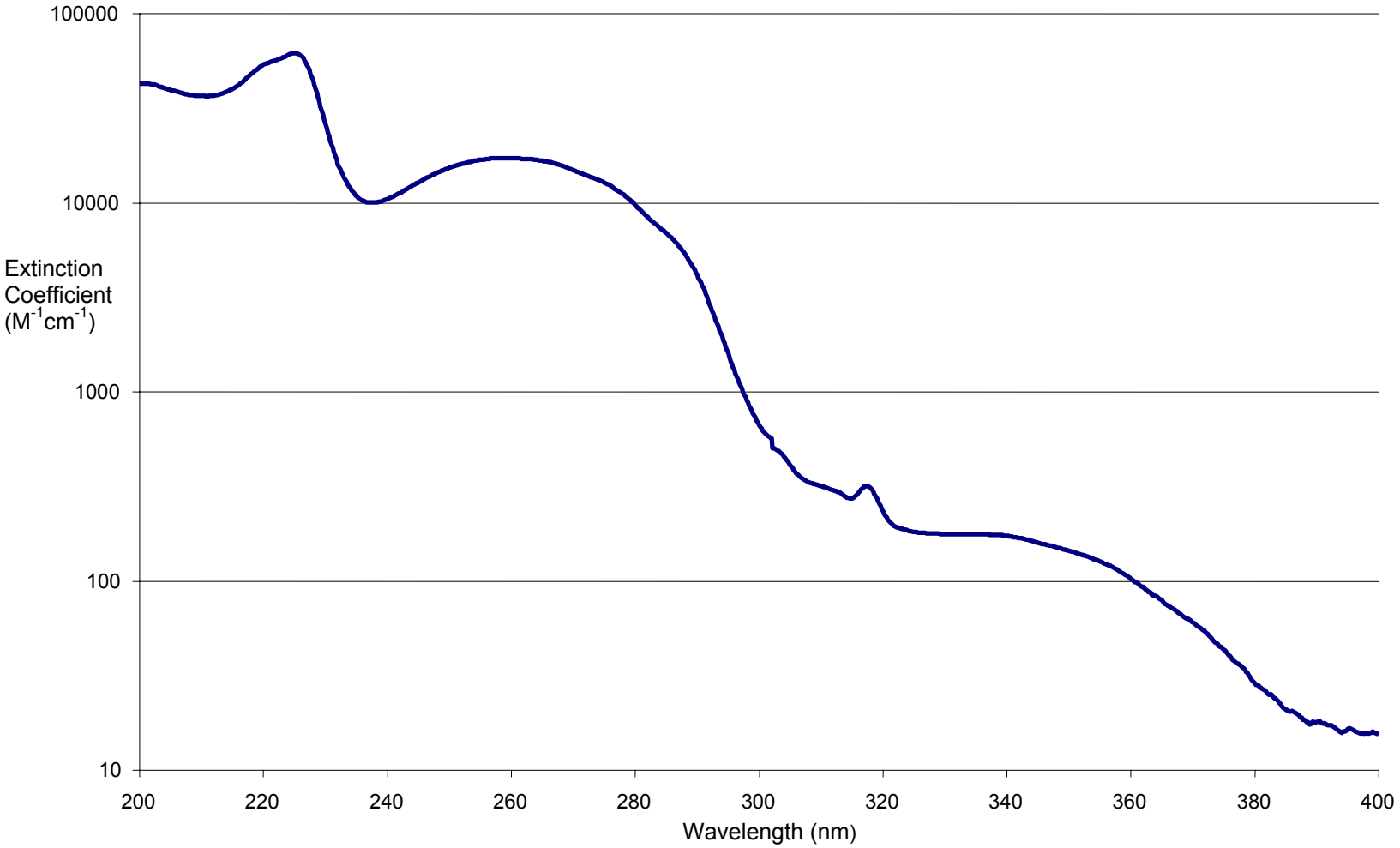

**Figure 11: Extinction coefficient plot for 1B**

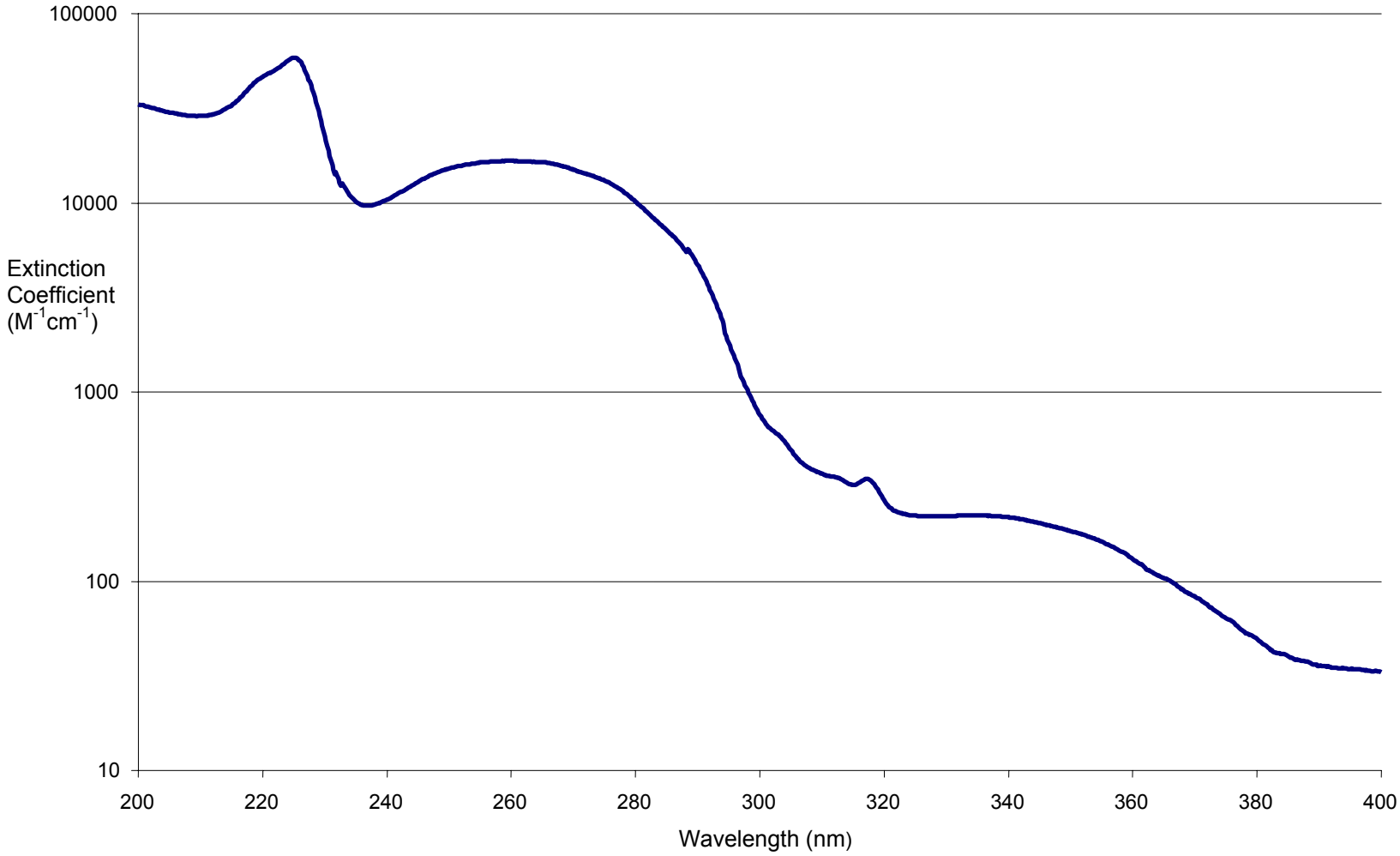

**Figure 12: Fluorescence Spectra of Boc-2-Nal-OH, 1A and 1B at an excitation wavelength of 224 nm**

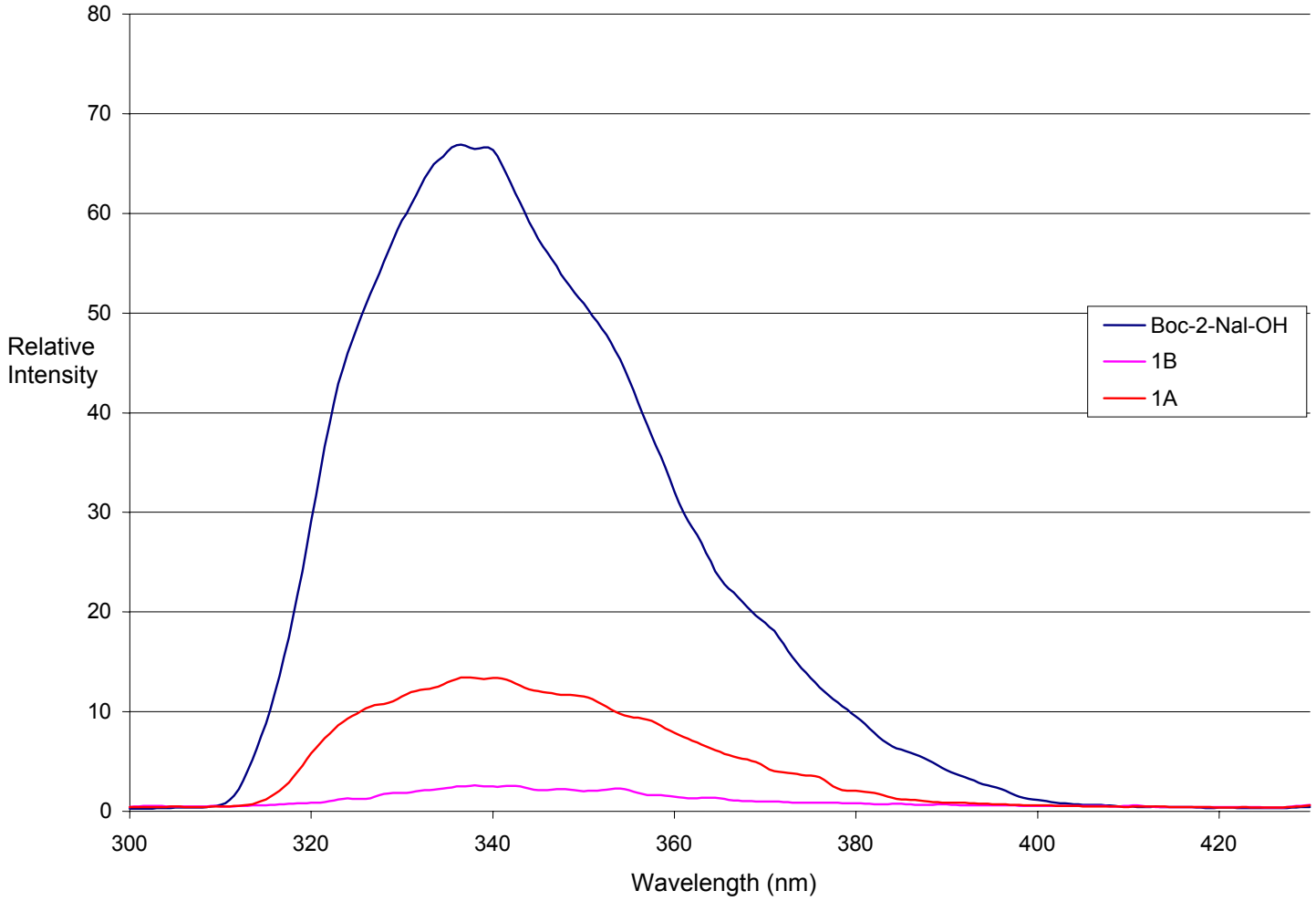

**Figure 13: Fluorescence spectra of Boc-2-Nal-OH, 1A and 1B at an excitation wavelength of 266 nm**

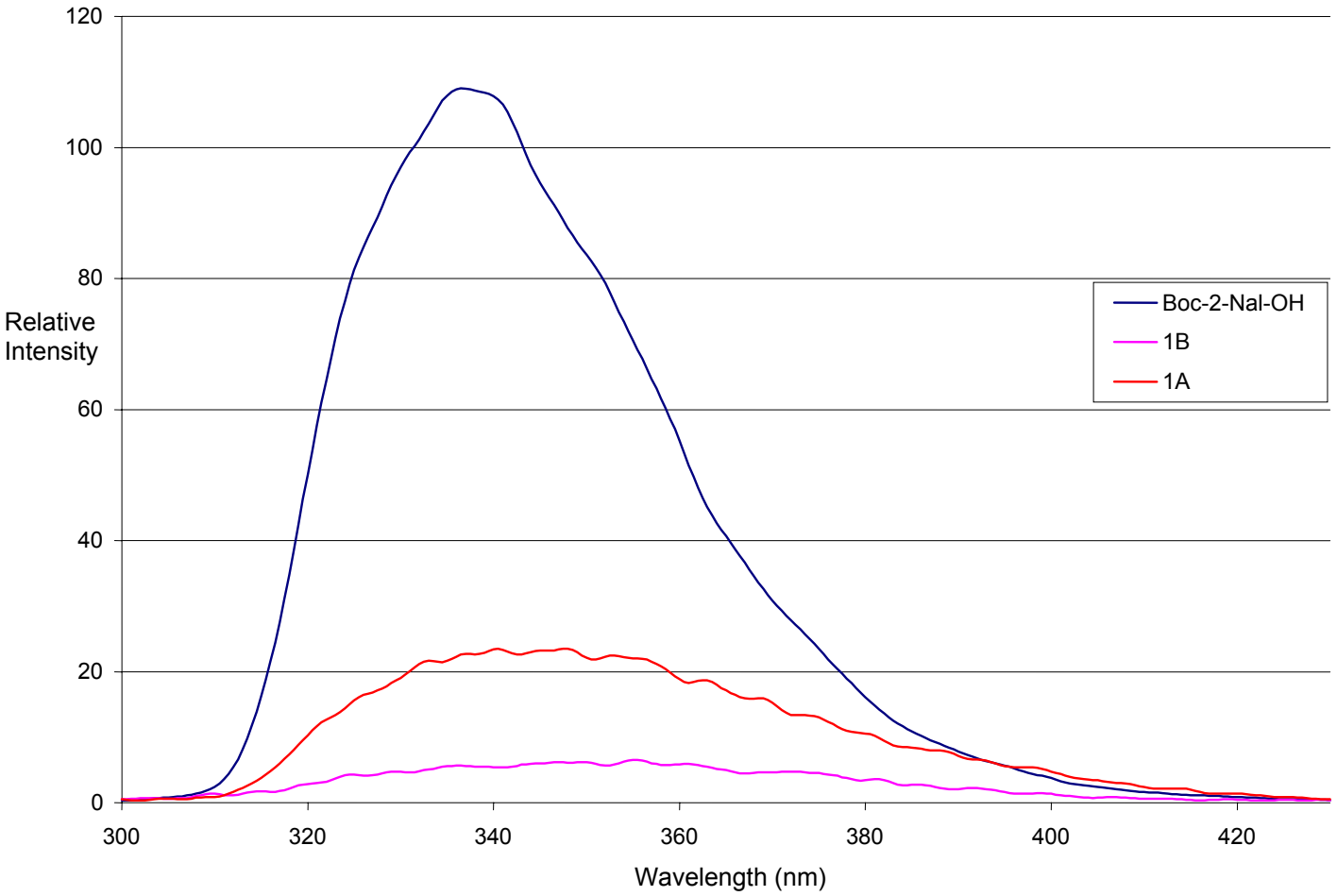

**Figure 14: Fluorescence spectra of Boc-2-Nal-OH, 1A and 1B at an excitation wavelength of 280 nm**

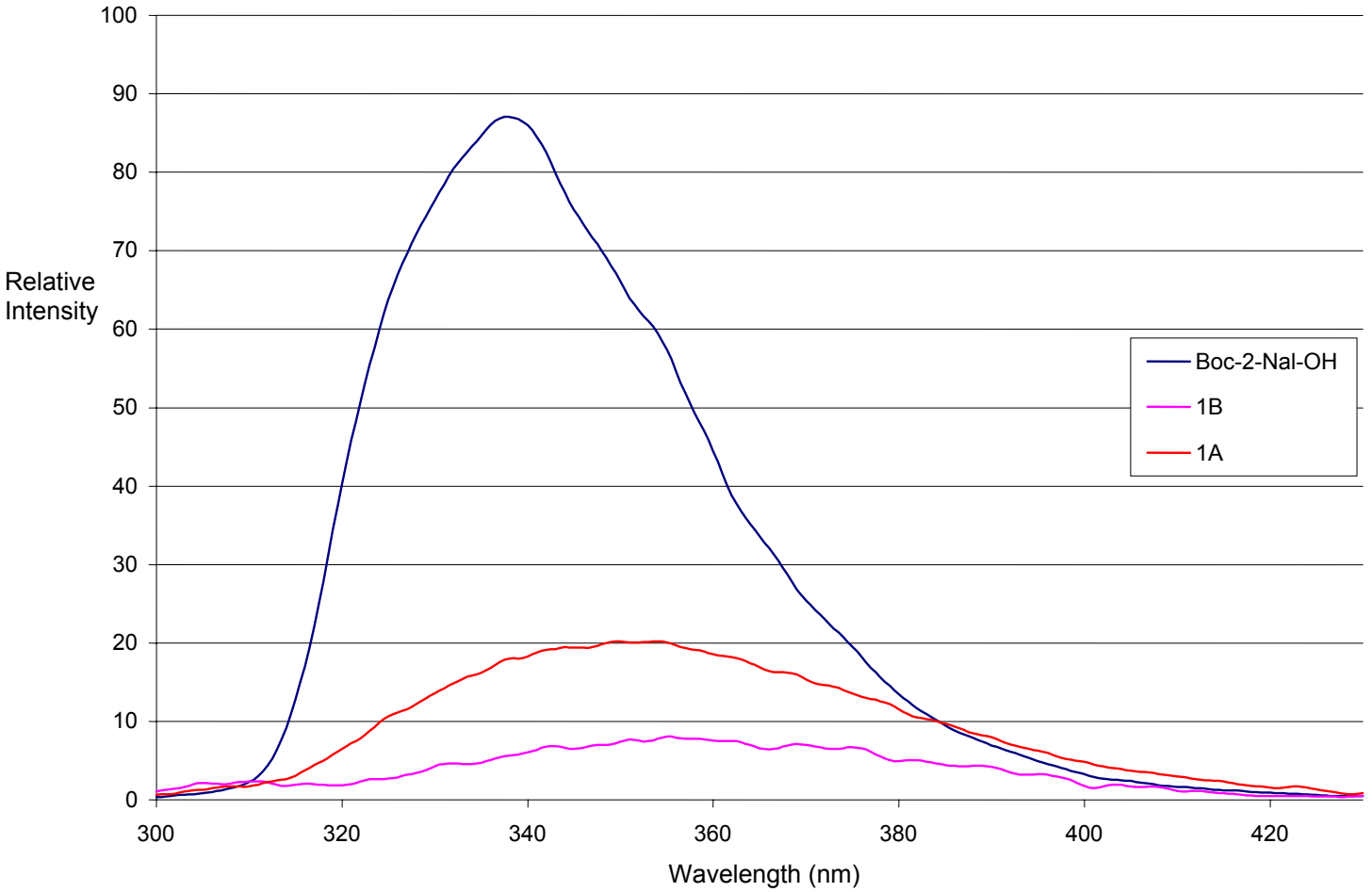

**Figure 15: Phosphorescence spectra of Boc-Bpa-OH, 1A and 1B at an excitation wavelength of 266 nm at 77 K in 1:1 Methanol:Ethanol**

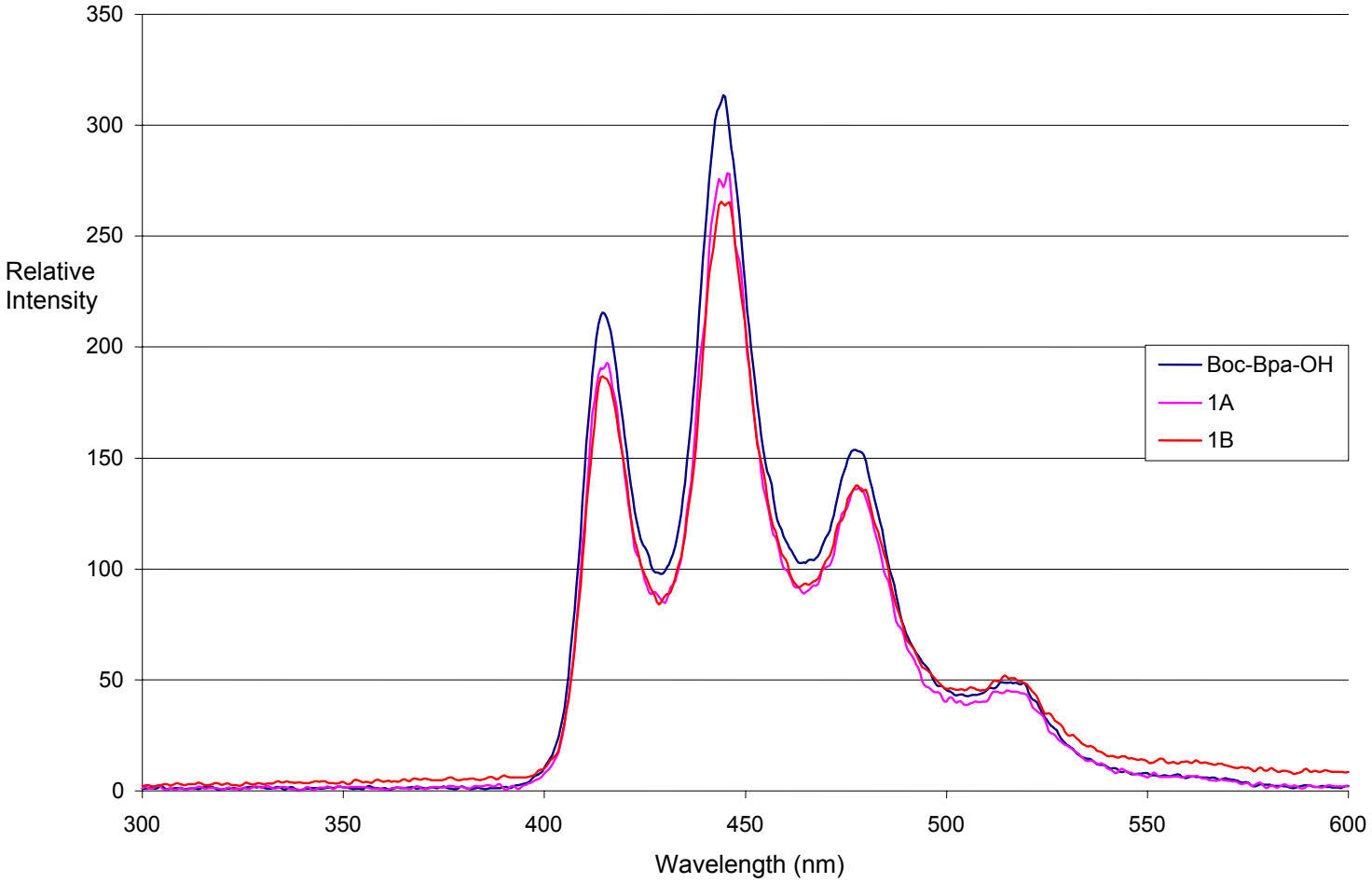

**Figure 16: Transient absorption spectra of Boc-Bpa-OH, Boc-2-Nal-OH, 1A and 1B at an excitation wavelength of 266 nm**

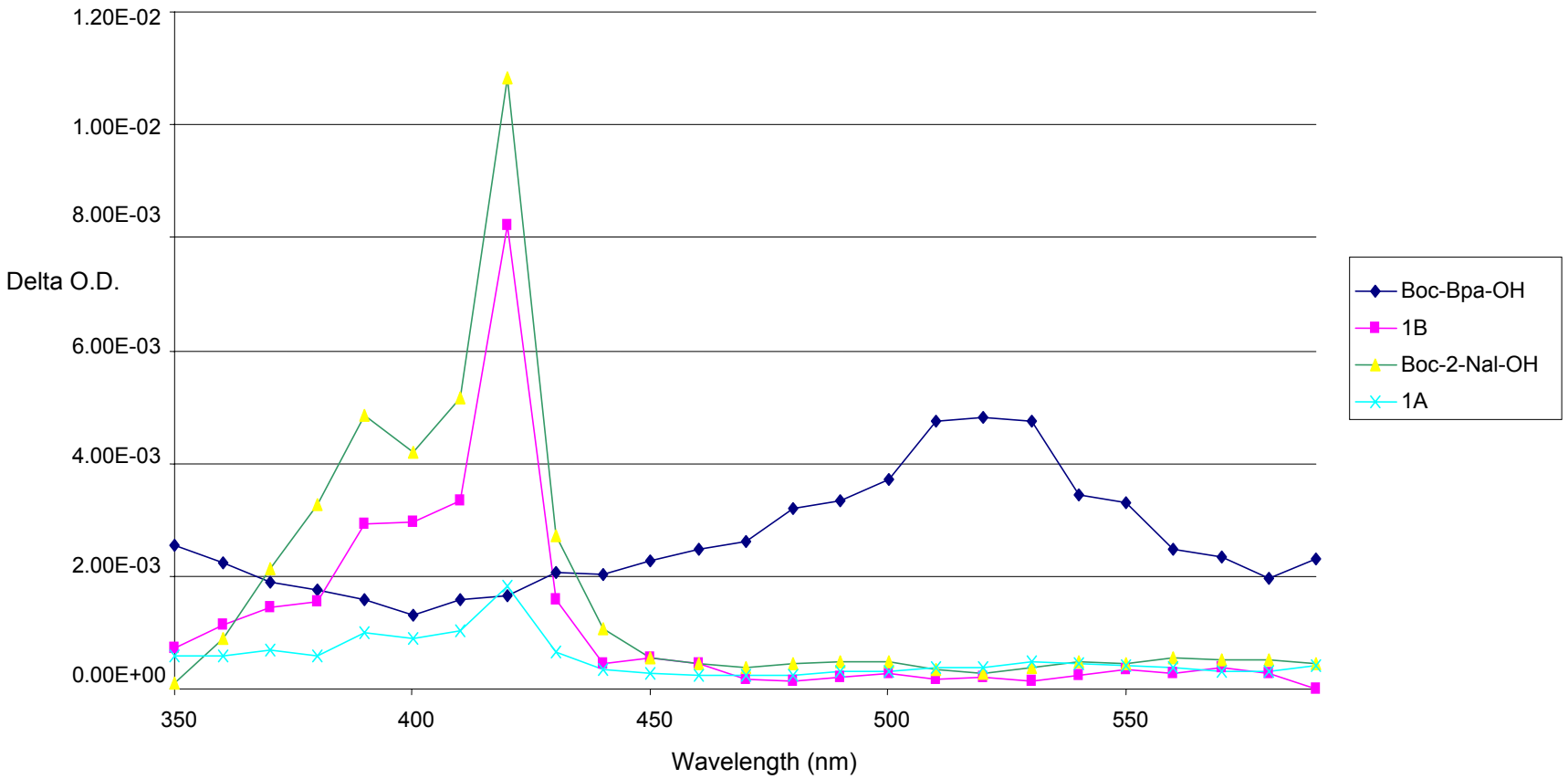

Spectroscopic results for compound 2A and 2B are shown in Figures 17-23.

Figure 17: Extinction coefficient plot for 2A

Figure 18: Extinction coefficient plot for 2B

Figure 19: Fluorescence spectra of Boc-2Nal-OH, 2A and 2B at an excitation wavelength of 224 nm

Figure 20: Fluorescence spectra of Boc-2Nal-OH, 2A and 2B at an excitation wavelength of 266 nm

Figure 21: Fluorescence spectra of Boc-2Nal-OH, 2A and 2B at an excitation wavelength of 280 nm

Figure 22: Phosphorescence spectra of Boc-Bpa-OH, 2A and 2B at an excitation wavelength of 266 nm

Figure 23: Transient absorption spectra of Boc-2Nal-OH, Boc-Bpa-OH, 2A and 2B at an excitation wavelength of 266 nm

**Figure 17: Extinction coefficient plot for 2A**

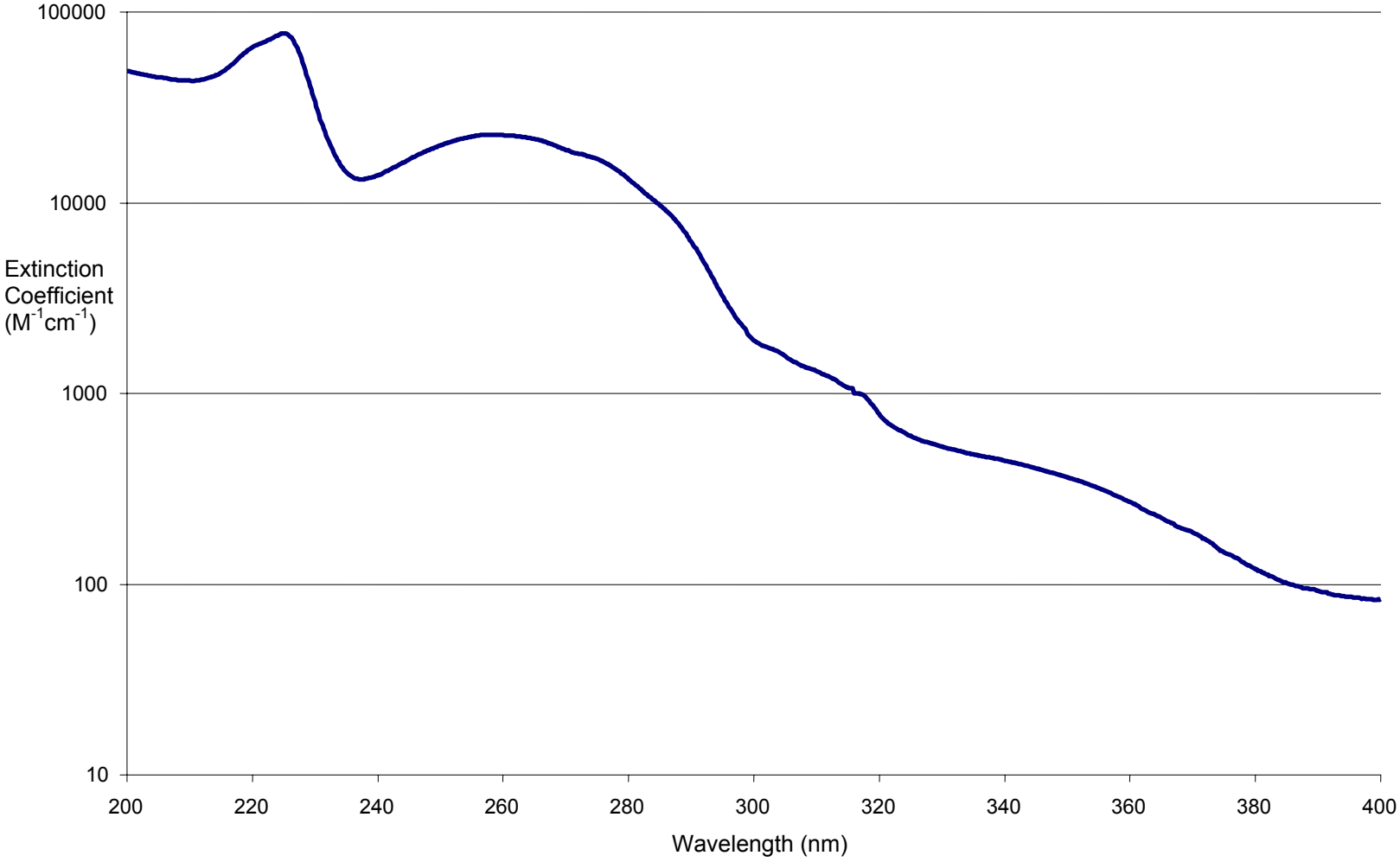

**Figure 18: Extinction coefficient plot for 2B**

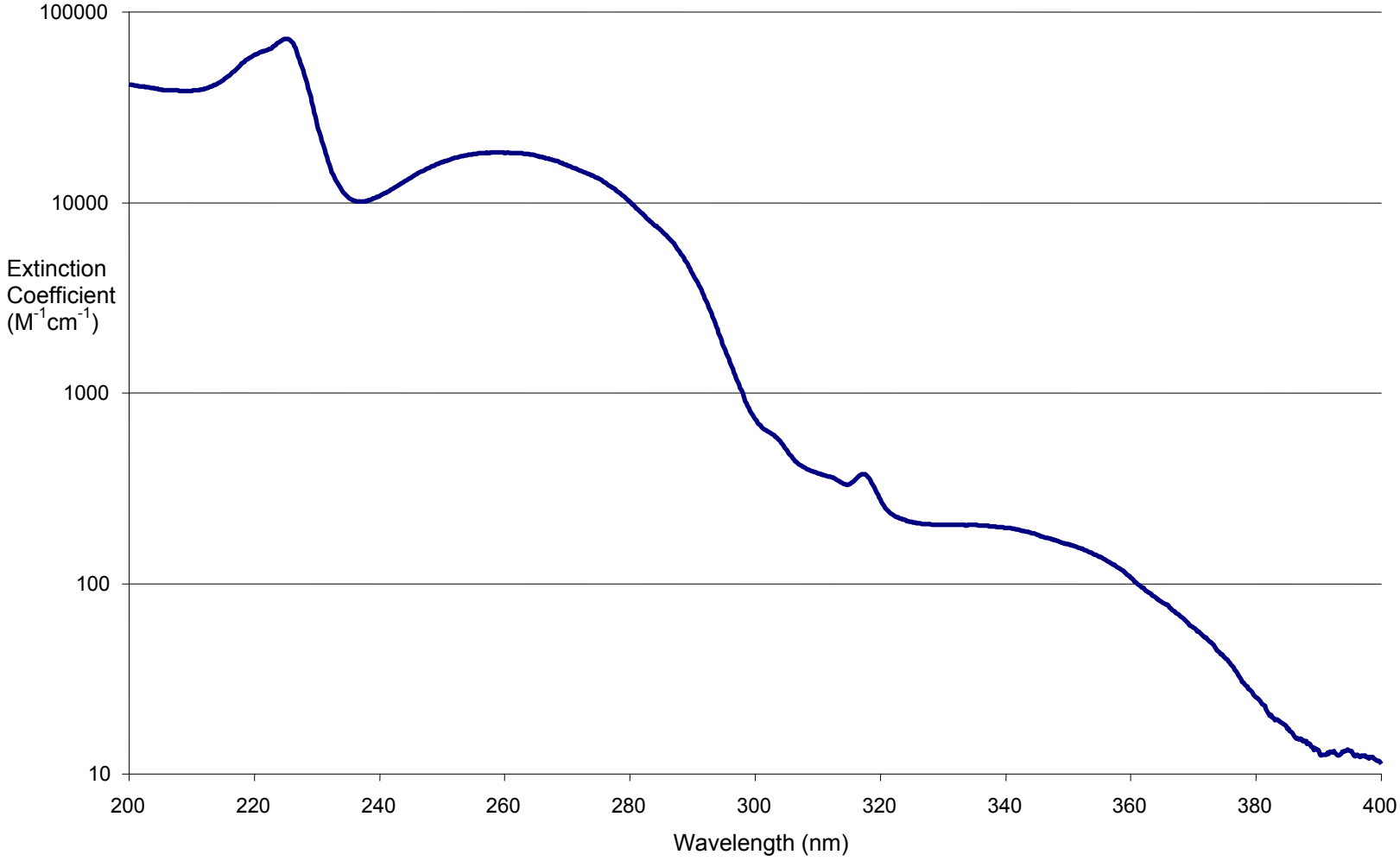

**Figure 19: Fluorescence spectra of Boc-2-Nal-OH, 2A and 2B at an excitation wavelength of 224 nm**

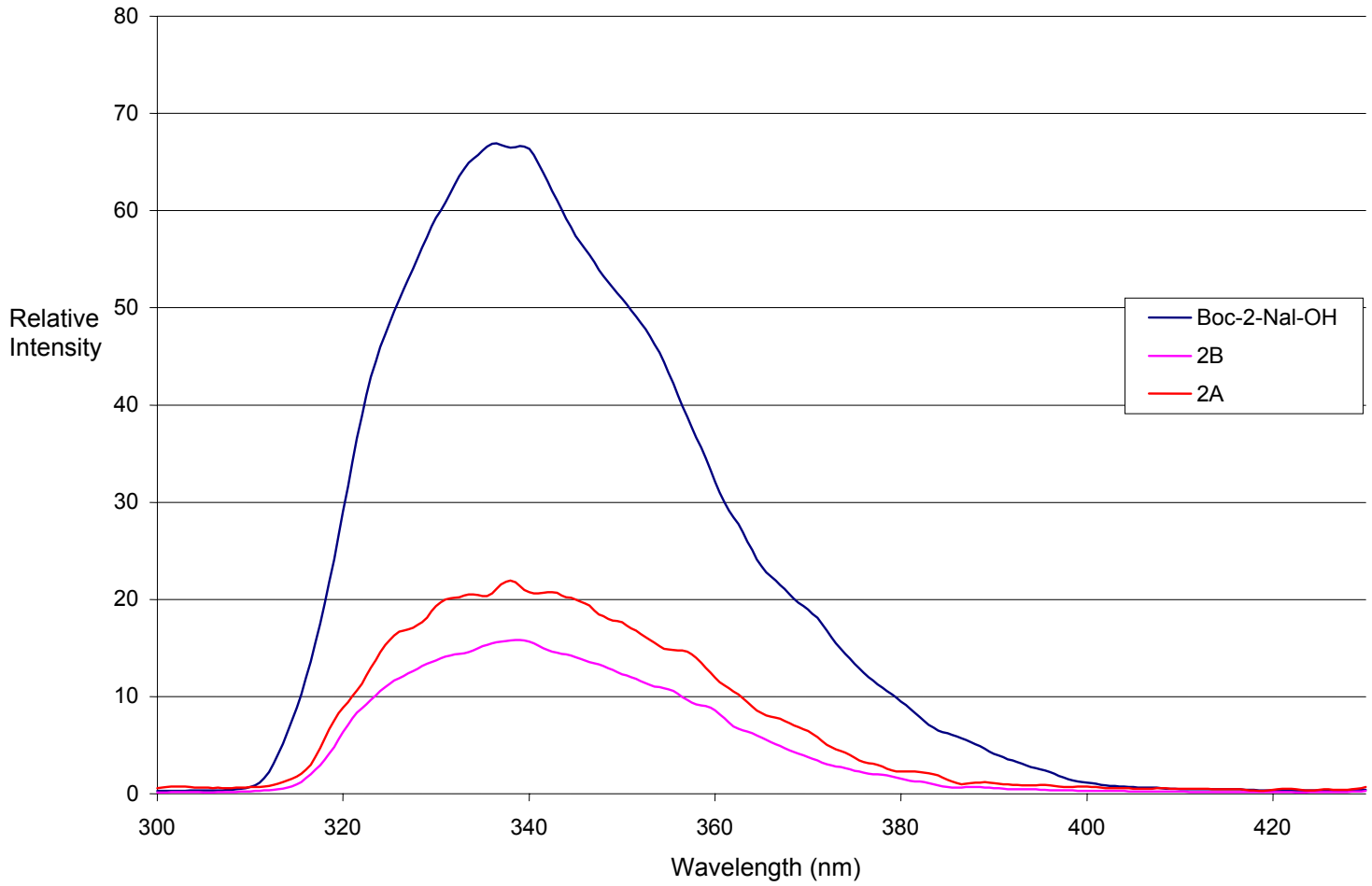

**Figure 20: Fluorescence spectra of Boc-2-Nal-OH, 2A and 2B at an excitation wavelength of 266 nm**

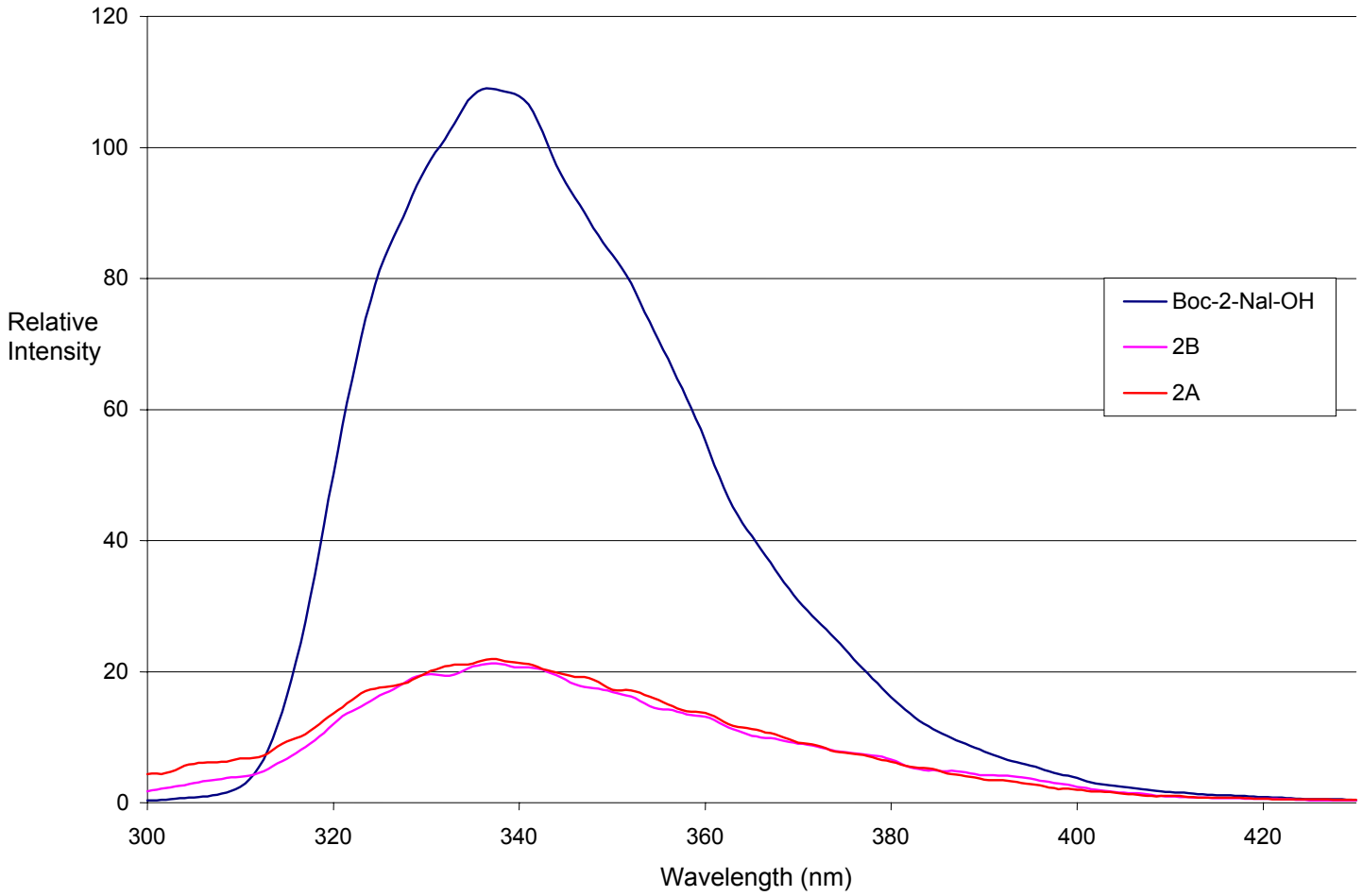

**Figure 21: Fluorescence spectra of Boc-2-Nal-OH, 2A and 2B at an excitation wavelength of 280 nm**

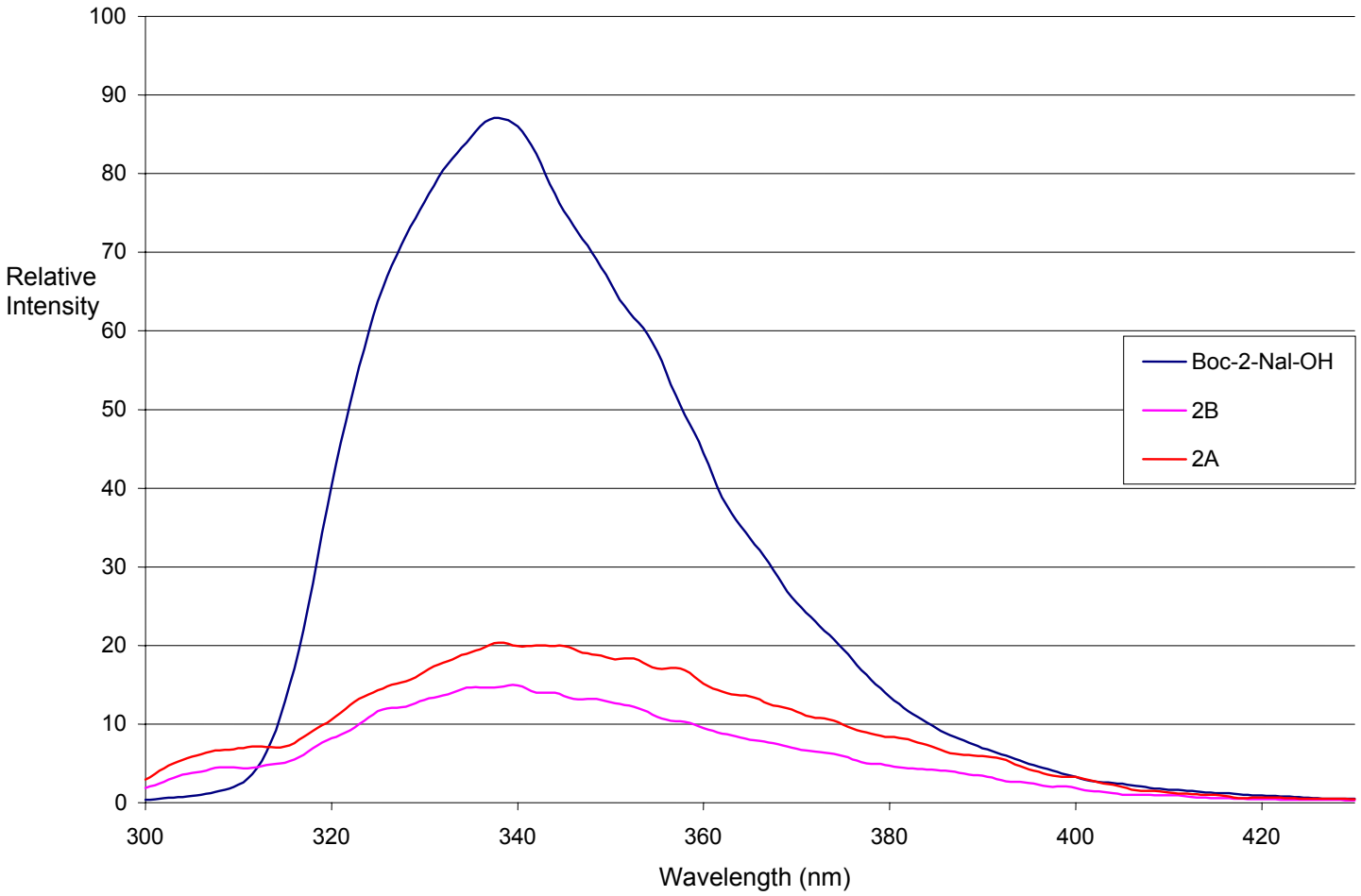

**Figure 22: Posphorescence spectra of Boc-BpaOH, 2A and 2B at an excitation wavelength of 266 nm at 77 K in 1:1 Methanol:Ethanol**

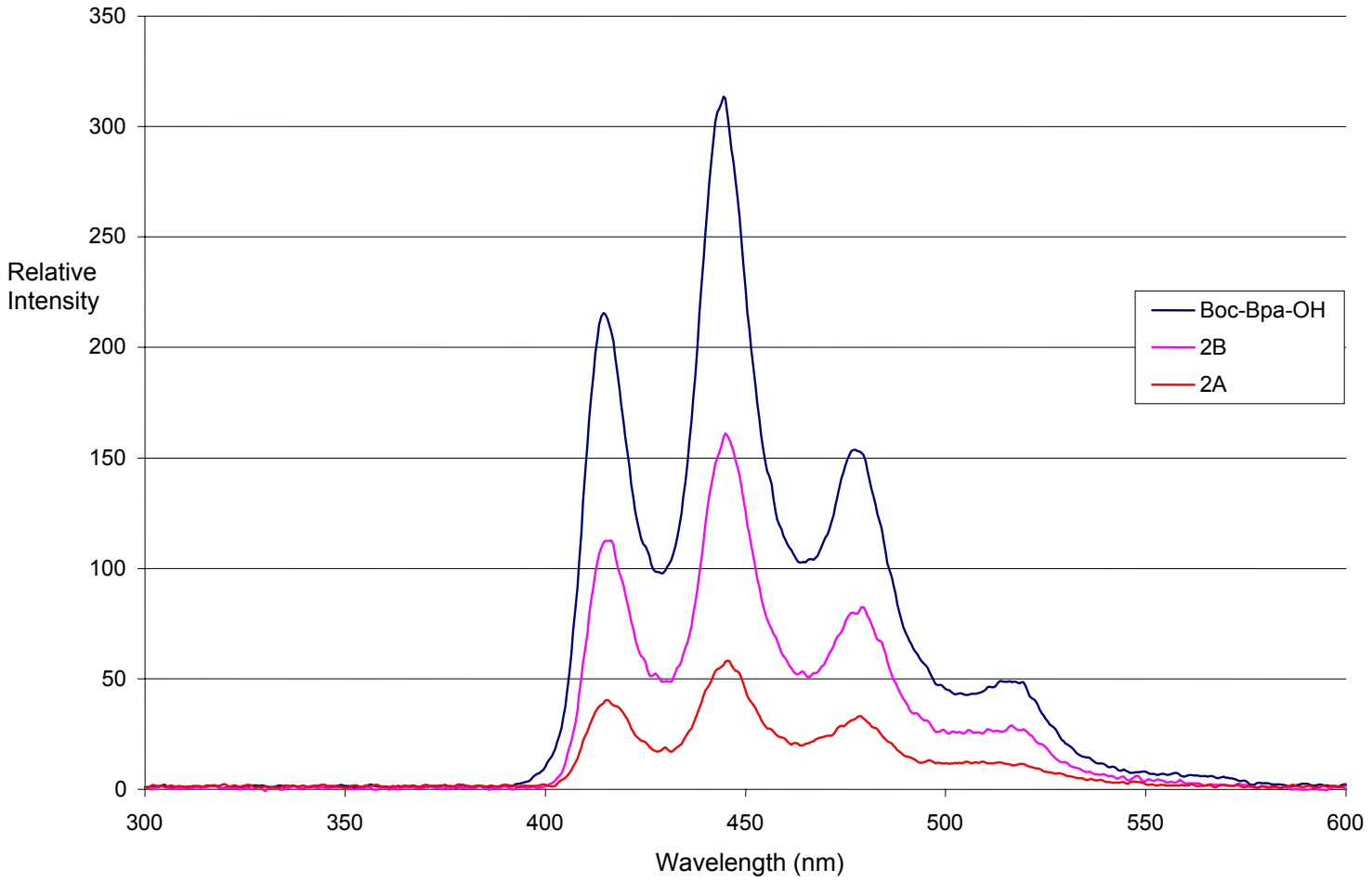

**Figure 23: Transient absorption spectra of Boc-Bpa-OH, Boc-2-Nal-OH, 2A and 2B at an excitation wavelength of 266 nm**

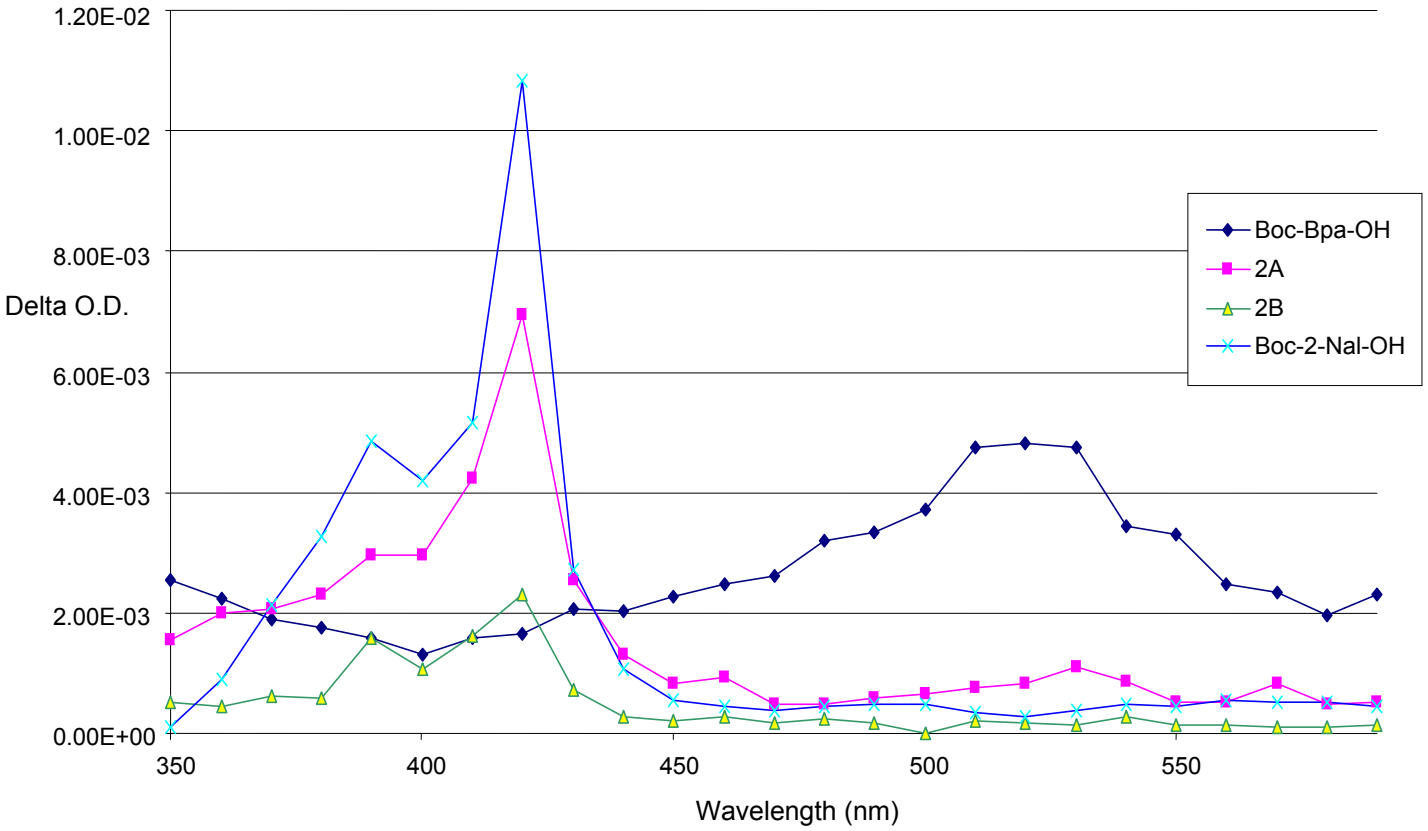

# Discussion

## Ground State Absorption Spectroscopy

t-Boc-3-(2-naphthyl)-L-alanine and t-Boc-(4-benzoyl)-L-phenyl alanine were used as model compounds for the naphthyl and benzophenone chromophores incorporated into the peptides studied. The t-Boc protected amino acids were used instead of the Fmoc protected analogs because the fluorene chromophore in the latter interferes with UV-visible absorption and fluorescence measurements. The sum of these spectra closely resembles the spectra of each of the open chain and cyclic peptides prepared in this study, indicating that there is likely little interaction between the chromophores in the ground state (Figures 8, 9, 10, 11,17 and 18). The only deviation observed is in the 200 nm – 220 nm region of the spectrum where presumably there is considerable absorption due to each of the amino acids in the peptide. These spectra indicate that the ground states of the peptides behave spectroscopically and electronically as the sum of two isolated chromophores. AM1 and ZINDO/S calculations further indicate that the highest energy occupied molecular orbitals and the lowest energy unoccupied molecular orbitals are localized on individual chromophores. Given these observations, it is likely that excitation

of the localized ground state of one of the chromophores initially will result in the production of an excited state that is also localized on the same chromophore. As a result, the ratio of extinction coefficients of Boc-2-Nal-OH and Boc-Bpa-OH at any given excitation wavelength can be taken as an accurate representation of the ratio of excited states for each chromophore initially formed upon excitation, i.e., before any redistribution of the energy by transfer processes. For example, we estimate that exposure of the peptides to an excitation wavelength of 224 nm will result in 94% of the excitation absorbed by the naphthalene chromophore and 6% by the benzophenone group. Figure 24 shows the ratio of extinction coefficients as initial excitation distributions for the two chromophores.

**Figure 24: Initial excitation distribution of Boc-2-Nal-OH and Boc-Bpa-OH**

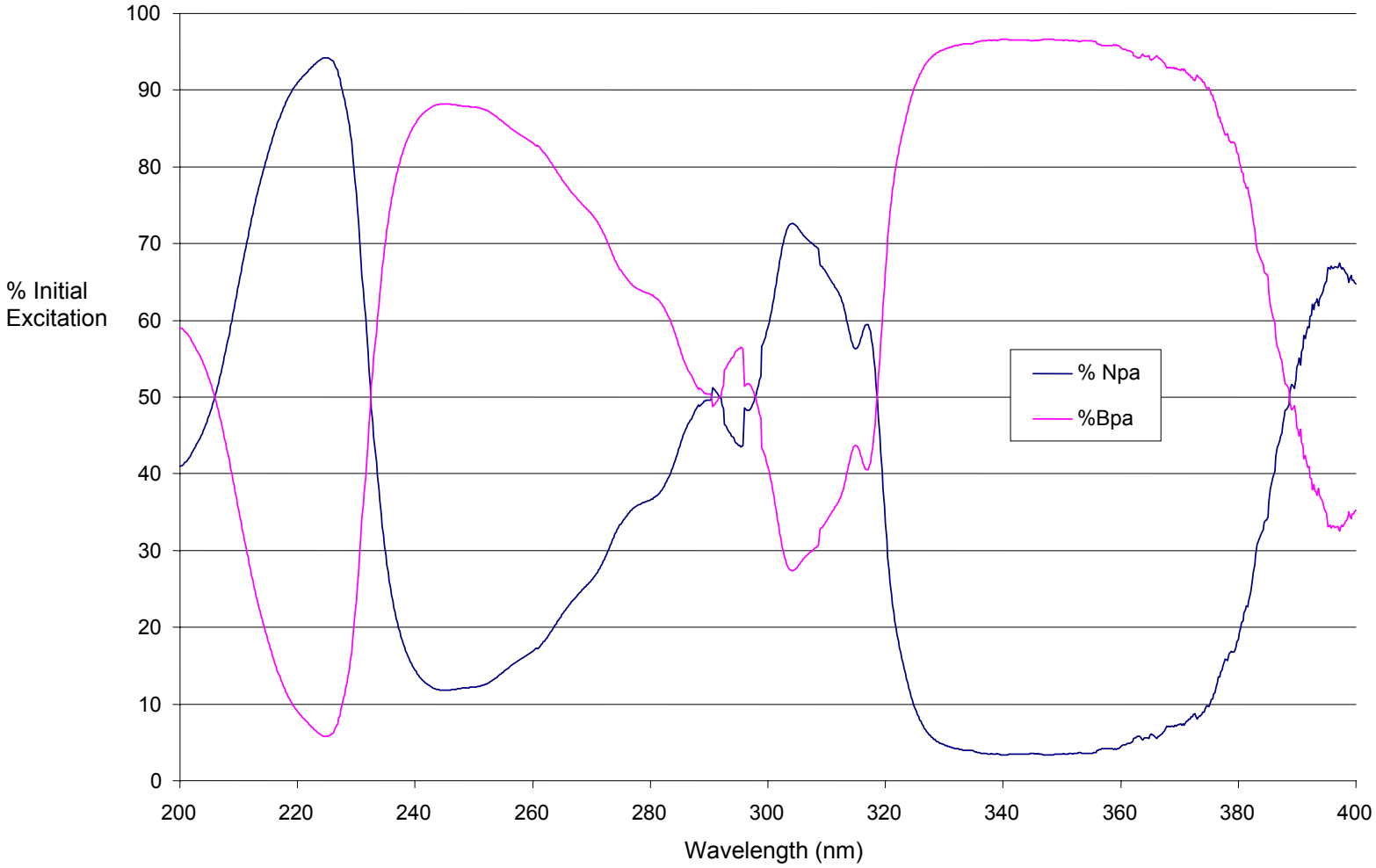

**Fluorescence Spectroscopy**

For fluorescence measurements, three different excitation wavelengths (224, 266 and 280 nm) were used. These excitation wavelengths correspond to quite different absorption conditions and were chosen to provide the maximum possible excitation of the naphthalene and benzophenone chromophores, respectively. Thus at 224 nm most of the incident light is absorbed by the naphthalene chromophore while at 266 nm the benzophenone group absorbs most strongly. At 280 nm, the extent of excitation is more comparable. Figures 12, 13, 14, 19, 20 and 21 show the emission spectra for Boc-2-Nal-OH and peptides obtained at those three different wavelengths. We note that at all of the excitation wavelengths used, the emission spectra for all of the peptides were identical in band shape to the spectrum of Boc-2-Nal-OH. This is not surprising given the non-emissive nature of the benzophenone singlet state. However, the emission intensity of the peptides was substantially less than for Boc-2-Nal-OH when the absorption of Boc-2-Nal-OH at the excitation wavelength was adjusted to match the absorption for the naphthyl chromophore in the peptides at that wavelength (as predicted from the extinction coefficient data). Results for each wavelength were quite similar for each of the peptides with the naphthalene chromophore emission intensity

undergoing attenuation by a factor of 3-5 depending on the peptide structure. These observations indicate that the naphthalene singlet state is quenched by the presence of the benzophenone group, likely as a result of SSET. This conclusion is based on the thermodynamic feasibility of SSET, results from phosphorescence and laser studies and on literature precedent, particularly McGimpsey and his group`s study of a bichromophoric α-helical open chain peptide containing benzophenone and naphthalene chromophores[11]. We conclude that this SSET quenching is intramolecular in nature since the concentration of the peptide used in the fluorescence experiments is too low ($<10^{-5}$ M), and the lifetime of the naphthyl singlet state as determined for naphthalene (~70 ns)[11] is too short to allow efficient intermolecular quenching.

The fluorescence intensity of naphthalene chromophore in the peptides is representative of the final excitation distribution in the molecule. The degree to which the emission intensity was attenuated in the peptides relative to Boc-2-Nal-OH can be used to calculate both an efficiency of SSET and a rate constant for this process ($k_{SSET}$). Equation 6 relates the experimentally obtained integrated fluorescence intensities for the peptides and Boc-2-Nal-OH to the rate constant for SSET ($k_{SSET}$). Here $I^F$ is the integrated fluorescence intensity, $k_F$ is the radiative rate constant for the

naphthalene chromophore and is assumed to be the same for Boc-2-Nal-OH and all of the peptides, $k_{All}$ is the sum of the rate constants for all intrachromophore deactivation processes including $k_F$, $k_{IC}$, $k_{ISC}$ and is equivalent to the rate constant obtained previously by fluorescence lifetime measurements on Boc-2-Nal-OH, and $k_{SSET}$ is the SSET rate constant. Table 1 gives values calculated from equation 6 for each of the peptides studied.

$$\frac{I^F_{peptide}}{I^F_{Boc\text{-}2\text{-}Nal\text{-}OH}} = \frac{ED_{Final}}{ED_{Initial}} = \frac{k_F / (k_{All} + k_{SSET})}{k_F / k_{All}} = \frac{k_{All}}{k_{All} + k_{SSET}} \quad \textbf{(6)}$$

Table 1: SSET and TTET rate constants for bichromophoric peptides

| Compound | $\lambda_{ex}$ (nm) | $E_{SSET}$ | $k_s$ of donor ($s^{-1}$) | $k_{SSET}$ ($s^{-1}$) | $k_{SSET}$($s^{-1}$) (Average) | $R_0$ (Å) | R (Å) | $R_{model}$(Å) (Average) | $E_{TTET}$ | $k_{TTET}$ ($s^{-1}$) |
|---|---|---|---|---|---|---|---|---|---|---|
| **1B** | 224 | 96.3 | $9.5x10^6$ | $2.44x10^8$ | $1.87x10^8$ | 14.7 | 9 | 9.5 | | |
| | 266 | 95 | | $1.8x10^8$ | | | | | 2.5 | $5x10^2$ |
| | 280 | 94 | | $1.36x10^8$ | | | | | | |
| | | | | | | | | | | |
| **1A** | 224 | 80 | $9.5x10^6$ | $3.8x10^7$ | $3.67x10^7$ | 14.7 | 11.8 | 14.1 | | |
| | 266 | 79 | | $3.6x10^7$ | | | | | 2 | $3.6x10^2$ |
| | 280 | 79 | | $3.6x10^7$ | | | | | | |
| | | | | | | | | | | |
| **2B** | 224 | 77 | $9.5x10^6$ | $3.1x10^7$ | $3.9x10^7$ | 14.7 | 11.9 | 6.5 | | |
| | 266 | 81 | | $3.9x10^7$ | | | | | 32 | $9.4x10^3$ |
| | 280 | 83 | | $4.7x10^7$ | | | | | | |
| | | | | | | | | | | |
| **2A** | 224 | 69 | $9.5x10^6$ | $2.1x10^7$ | $3x10^7$ | 14.7 | 12.2 | 8.1 | 74.3 | $5.7x10^4$ |
| | 266 | 80 | | $3.7x10^7$ | | | | | | |
| | 280 | 77 | | $3.2x10^7$ | | | | | | |

SSET is normally discussed in terms of Förster (dipole-induced dipole) and/or Dexter (electron exchange) mechanisms. When the energy transfer process is intramolecular, a super exchange process involving through-bond transfer may also be operative. This latter process is usually most effective when the molecular structure linking the chromophores is rigid and the bonds in the linker are *all-trans* although through-bond electron transfer has been observed in bichoromophoric molecules employing other linkers, including amides and peptides.

The most straightforward intramolecular mechanism to evaluate is the Förster mechanism. In general, the efficiency of Förster energy transfer is given by equation 7 where $R_0$ is the critical Förster separation, the donor/acceptor distance at which the rates of energy transfer and the intrinsic deactivation of the donor excited state in the absence of the acceptor are the same, i.e., 50% transfer efficiency (calculated according to equation 2 from the introduction and reproduced here as equation 8), and R is the actual interchromophore separation assuming that Förster transfer is the dominant transfer mechanism.[5h]

$$E_{SSET} = \frac{1}{1 + \frac{R^6}{R_0^6}} \qquad \textbf{(7)}$$

$$R_0^6 = \frac{9100(\ln 10)\Phi_D \kappa^2}{128\eta^4 \pi^5 N_A} J \qquad \textbf{(8)} \qquad J = \frac{\int_0^\infty f_D(\nu)\varepsilon_A(\nu)\nu^{-4} d\nu}{\int_0^\infty f_D(\nu)}$$

Evaluation of the importance of the Förster transfer mechanism in the peptides studied involves determination of the SSET efficiency from fluorescence measurements, calculation of the critical Förster distance from spectroscopic data and equation 8, and the use of equation 7 to obtain a value for R. Comparison of this interchromophore separation with that obtained by molecular modeling gives a qualitative evaluation of the importance of Förster transfer. The transfer efficiency can be calculated from equation 9.

$$E_{SSET} = 1 - E_F \qquad \textbf{(9)}$$

Table 1 contains values of $R_0$ and R for each of the peptides as well as interchromophore separations as determined by molecular modeling and dynamics calculations. As we have studied above, one of the primary reasons for utilizing the cyclic peptide structure

is to obtain more rigid structures and in the process limit the range of interchromophore separations presented. The modeling studies appear to confirm that this is indeed the outcome for 1A and 2A. In the former, where the two chromophores nominally occupy positions on opposite sides of the cyclic peptide structure, an ensemble of minimum energy conformations yield interchromophore separations in a narrow range centered at 14.1 Å. In 2A, the chromophores occupy positions at $90^0$ to each other on the cyclic peptide and are expected to be closer to one another than in 1A. The interchromophore separation in 2A also has a narrow range, in this case centered at 8.1 Å. A strict Förster treatment of the data for 1A and 2A does not provide a conclusive explanation of the energy transfer behavior. The critical Förster distance in 1A is 3 Å less than the distance predicted by modeling while in 2A the predicted separation is 4 Å less than the critical distance. For 1A, then, SSET appears to be more efficient than predicted by Förster while in 2A it appears to be less efficient. We do not have a definitive explanation for this apparent inconsistency. It is possible that in our modeling studies we were not able to fully explore the energy surface and as a result omitted other low energy conformations. However, we *have* been able to reproduce the suggestion by Ghadiri et al. that cyclic peptides incorporating α-amino-iso-butyric acid residues lose their β-conformations in favor

of helical structures.[14] In other words the cyclic peptide ring is not disk-like, but puckered. The modeling results appear to confirm this suggestion. Another possibility is that SSET occurs by the exchange or superexchange mechanisms (with efficiencies that vary from 1A to 2A) in addition to the Förster mechanism. We are continuing our computational studies on these structures.

The open chain peptides 1B and 2B also show deviations from strict Förster behavior. In these cases, greater conformational freedom can be applied with more certainty as a potential source of the inconsistencies.

In the following figures 25, 26, 27 and 28 structures of the peptides obtained from molecular modeling studies are shown. Modeling was performed using MOE, and minimized using the Amber94 force field under conditions simulating *in vacuo* and in a bulk dielectric equal to that of acetonitrile.

Figure 25: Molecular Modeling structure of 1A

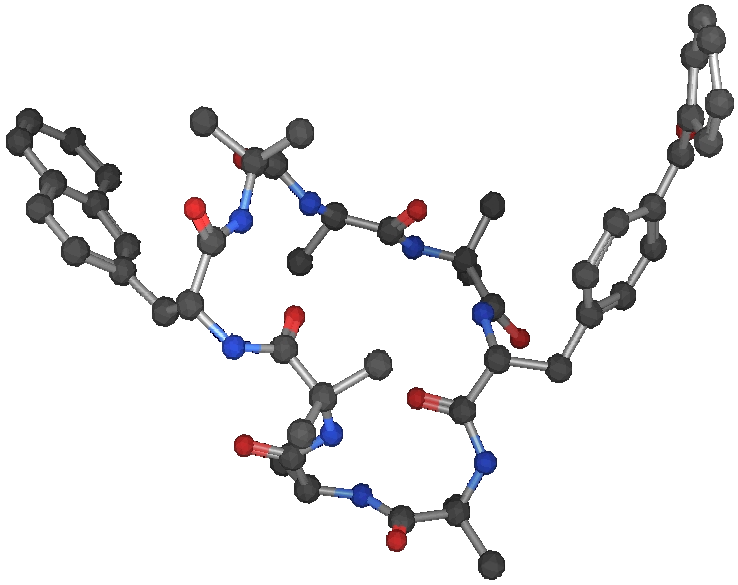

Figure 26: Molecular Modeling structure of 1B

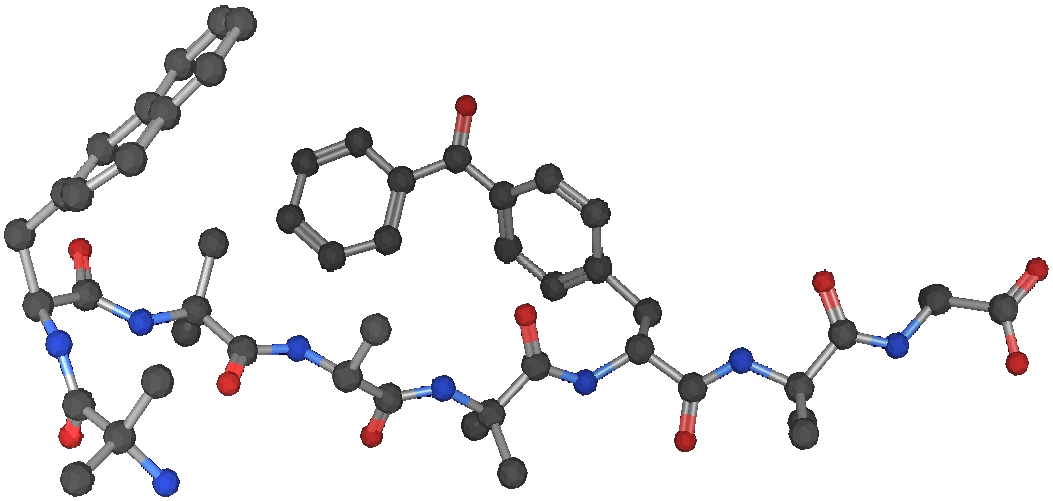

Figure 27: Molecular Modeling structure of 2A

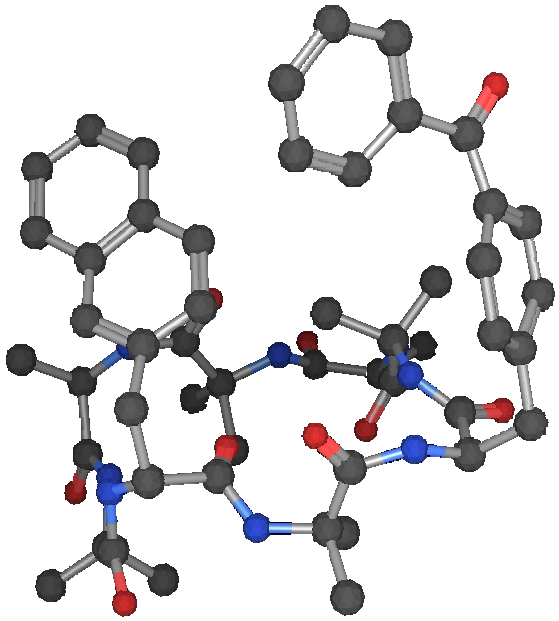

Figure 28: Molecular Modeling structure of 2B

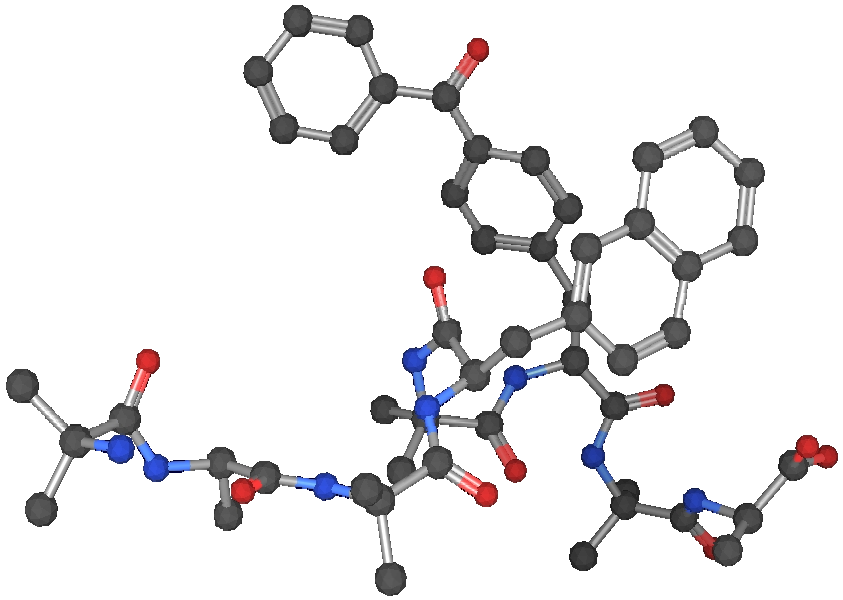

**Phosphorescence Spectroscopy**

The phosphorescence spectra of Boc-Bpa-OH, 1A, 1B, 2A and 2B are shown in figures 15 and 22. All of the peptides were prepared in nitrogen saturated 1:1 Ethanol/Methanol solution at 77 K. Samples were excited at 266 nm where 77% of the light was absorbed by the benzophenone moiety. A wavelength at which the benzophenone group absorbs the majority of the excitation was chosen because TTET from benzophenone to naphthalene was expected. (If there is no benzophenone absorption at the excitation wavelength then it would be difficult to measure the extent of TTET.) The triplet energies of benzophenone and naphthalene are 69.2 kcal/mole and 61.2 kcal/mole respectively.[16] Therefore TTET is thermodynamically favorable from benzophenone to naphthalene moiety.

By comparing the spectral shape of the model Boc-Bpa-OH and the peptide phosphorescence emissions, it is possible to conclude that TTET occurs from benzophenone to naphthalene. 1B, 1A and Boc-Bpa-OH have similar phosphorescence emissions. However in 2B and 2A, remarkable quenching in the emission of benzophenone was observed, we attribute this to energy transfer from the triplet state of benzophenone to the triplet state of naphthalene. The energy transfer efficiency ($E_{TTET}$) can be estimated from the

quenching rate of benzophenone phosphorescence emission. $E_{TTET}$ in 2A is about 75% in the glass matrix. Diffusional interaction is not expected to occur in the glass matrix because of the low temperature experiment and therefore the quenching of the benzophenone triplet state is likely due to an intramolecular process. A similar analysis for other peptides was performed and the data are given in Table 1. The phosphorescence emission intensity of the benzophenone chromophore in the peptides is representative of the final excitation distribution in the molecule. The degree to which the emission intensity was attenuated in the peptides relative to Boc-Bpa-OH can be used to calculate both an efficiency of TTET and a rate constant for this process ($k_{TTET}$).

However, according to the time resolved laser results (see below), it is clear that the actual rate for the TTET is larger than calculated values.

For 2B, quenching of the phosphorescence emission is less than in 2A. It is likely that the less efficient TTET is due to the glass matrix limiting access to conformations that are required for efficient energy transfer. Relative conformational freedom in 2B could result in less orbital overlap between the chromophores than in 2A.

The phosphorescence spectra of 1B and 1A are very similar to the Boc-Bpa-OH phosphorescence emission indicating that TTET is relatively inefficient for these peptides. However these results are inconsistent with the room temperature time resolved laser spectroscopy measurements, in which rapid intramolecular TTET can be observed. The reason for these different observations could be the result of more rotational mobility at room temperature than the low temperature matrix. The low temperature matrix may freeze or restrict the motion of chromophores and as a result of good orbital overlap of the chromophores may be prevented. Therefore it can be concluded that smaller interchromophore distances provide more TTET. However, at the same time a small distance between the chromophores may result in a large variety of conformations having good or poor orbital overlap.

The TTET rate constants calculated are the minimum rates for the energy transfer rates shown in table 1.

**Laser Flash Photolysis**

Figures 16 and 23 show the transient absorption spectra of Boc-2-Nal-OH, Boc-Bpa-OH, 1A, 1B, 2A and 2B. All of the samples were excited at 266 nm with a Nd-YAG laser in acetonitrile under

nitrogen saturated conditions. At this excitation wavelength the benzophenone moiety absorbs 77% of the incident light.

Kinetic data obtained for the compounds under nitrogen-saturated and air-saturated conditions show that the transient spectra were remarkably quenched by oxygen. This is evidence for triplet state formation. TTET is thermodynamically favorable from benzophenone to naphthalene because of the higher triplet state energy of benzophenone. Although most of the light was absorbed by benzophenone, naphthyl triplet formation was observed after the excitation of peptides by 266 nm YAG laser and no benzophenone triplet was observed, confirming TTET.

Since no resolvable growth kinetics were observed, energy transfer is not expected to be intermolecular. However intersystem crossing from the naphthalene singlet state to the triplet state could be an additional factor for formation of the naphthyl triplet.

These laser data combined with the phosphorescence results confirm that TTET occurs in the cyclic peptides and the efficiency of this process appears to be correlated with the interchromophore separations as determined by our modeling calculations.

## Conclusions

Ground state absorption spectroscopy, fluorescence, phosphorescence and laser flash photolysis have been used to study SSET and TTET processes for open chain and cyclic peptides. SSET and TTET occur efficiently for 2B and 2A. According to the fluorescence and phosphorescence emission experiments, only efficient SSET was observable for 1B and 1A. However, room temperature transient absorption experiments showed possible TTET for 1A and 1B.

Förster critical distance calculations and molecular modeling studies indicate that the dipole-induced dipole mechanism is the most efficient mechanism for SSET. However there is the possibility to have electron exchange especially because interchromophore separations are sufficiently small to allow this process.

The estimated energy diagrams for the bichromophoric peptides are given in the figures 29, 30, 31 and 32.

## Energy diagrams

Figure 29: Energy diagram for 1A

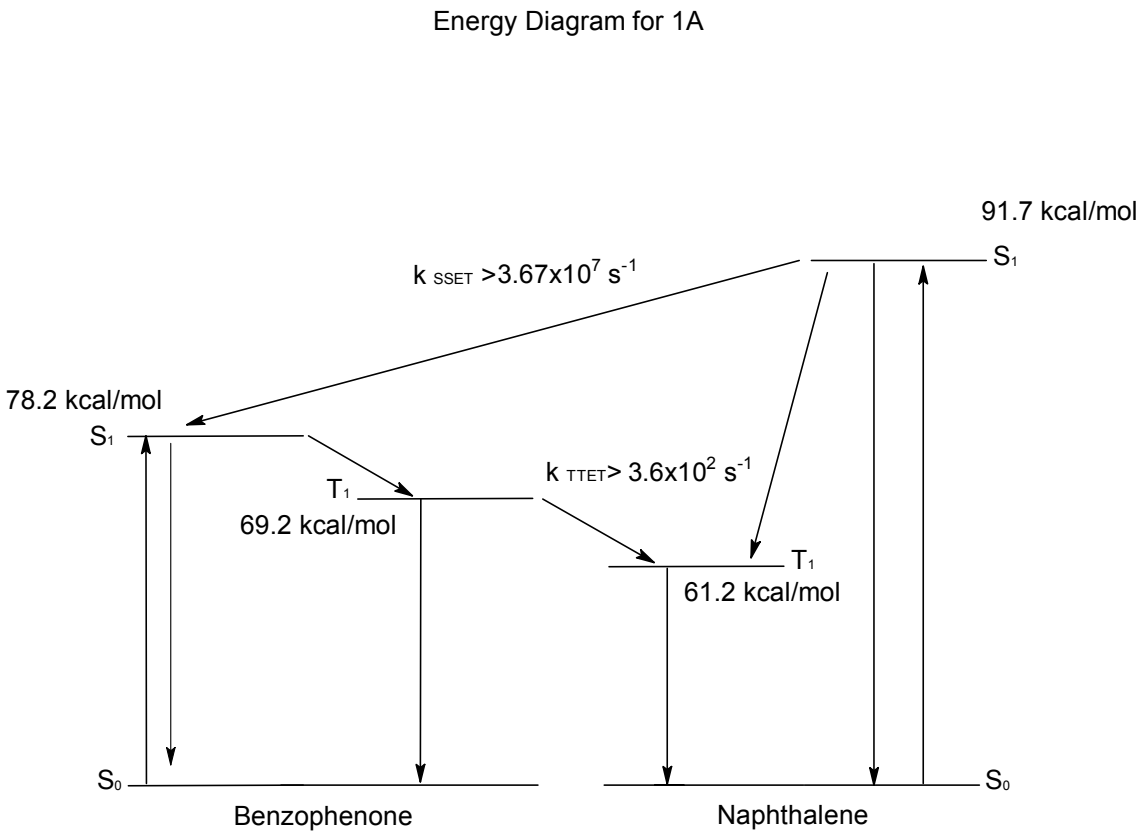

Figure 30: Energy diagram for 1B

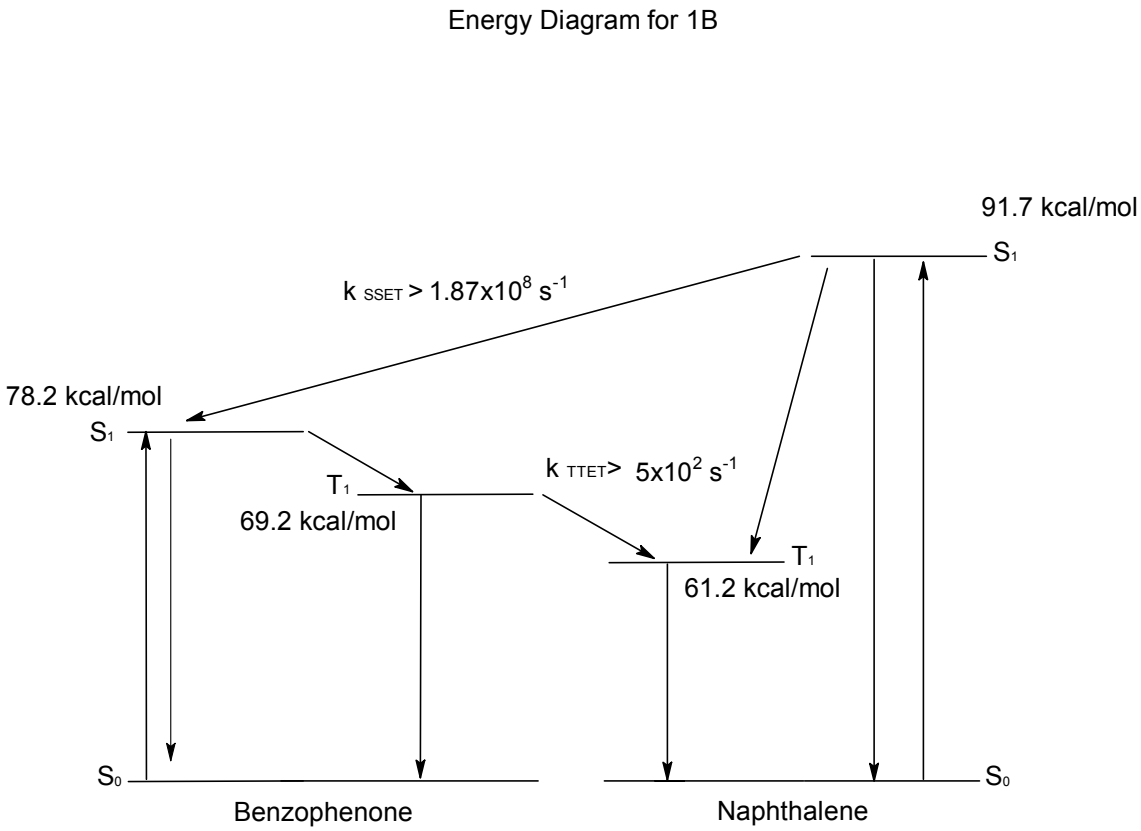

Figure 31: Energy diagram for 2A

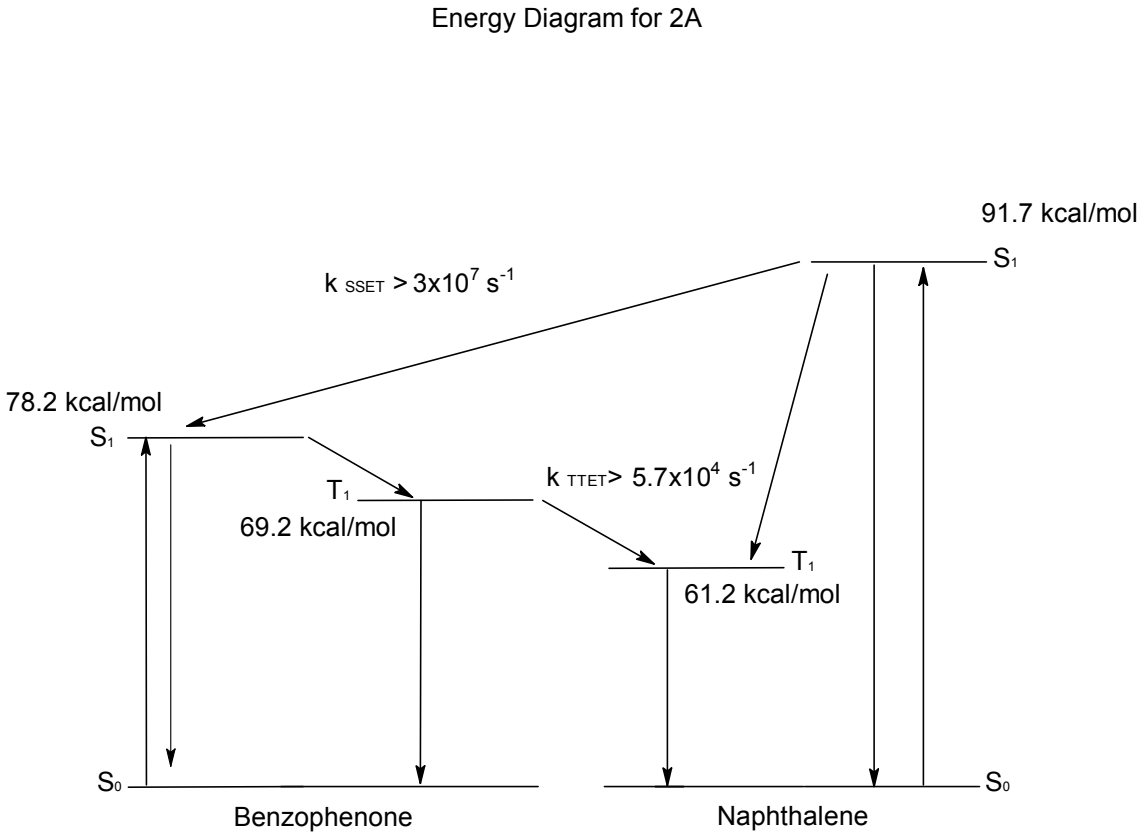

Figure 32: Energy diagram for 2B

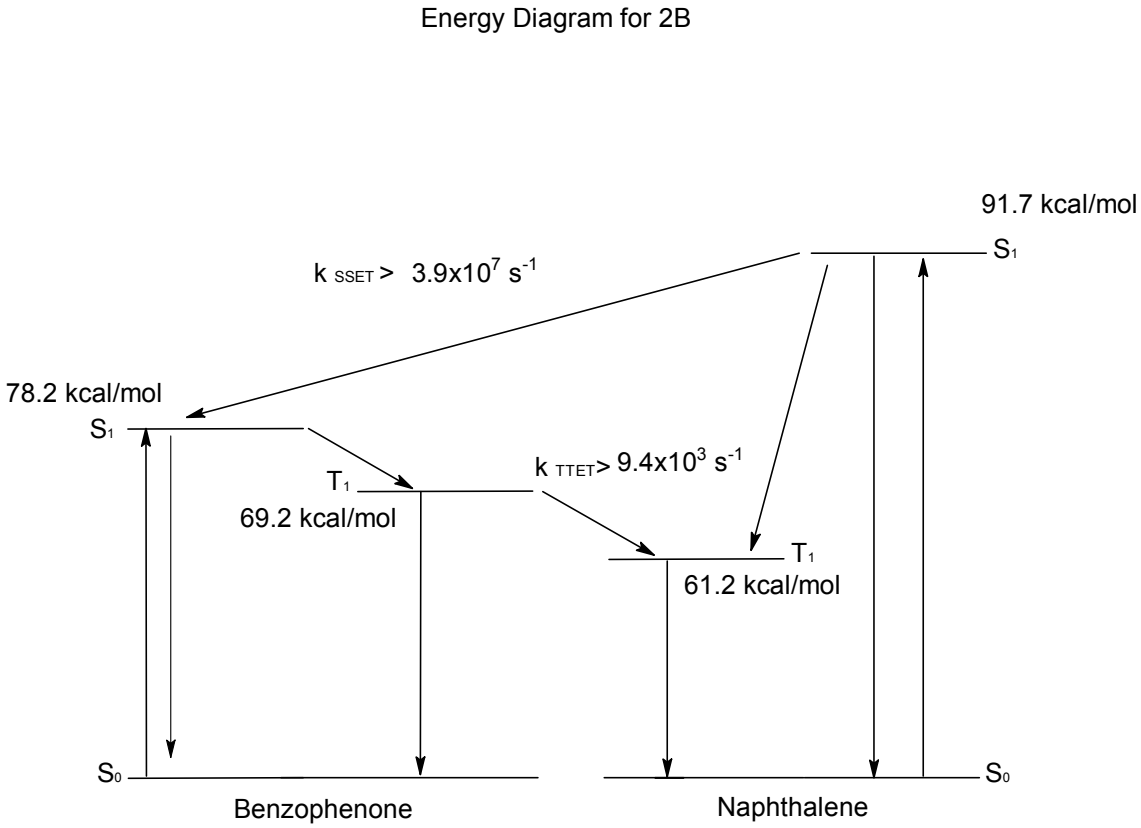

## References


1)

a) Tour, J.M. Acc. Chem. Res. 2000, 33, 791-804.)(Wagner, R.W. ; Lindsey, J.S. *J. Am. Chem. Soc*. **1994**, 116, 9759.

b) Wagner, R.W. ; Lindsey, J.S. *J. Am. Chem. Soc*. **1994**, 116, 9759.

2)

a) Wagner,R.W. ; Lindsey, J.S. ; Seth, J. ; Palaniappan, V. ; Bocian, D. *J. Am. Chem. Soc.* **1996**, 118, 3996-3997.

b) Silva, A. P. ; Dixon, I.M. ; Gunaratne, H.Q.N. ; Gunnlaughsson, T. ; Maxwell, P.R.S. ; Rice, T.E. *J. Am. Chem. Soc*. **1999**, 121, 1393.

3)

a) Otsuki, J. ; Tsujino, M. ; Iizaki, T. ; Araki, K. ; Seno, M. ; Takatera, K. ; Watanabe, T. *J. Am. Chem. Soc*. **1997**, 119, 7895.

b) Walz, J. ; Ulrich, K. ; Port, H. ; Wolf, H.C. ; Wonner, J. ; Effenberger, F. *Chemical Physics Letter* **1993**,213, 321.

c) Hush. N.S. ; Wong, A. T. ; Bacskay, G.B. ; Reimers, J.R. *J. Am. Chem. Soc.* **1990**, 112, 4192.

d) Deans, R. ; Niemz, A. ; Breinlinger, E.C. ; Rotello, V. M. *J. Am. Chem. Soc.* **1997**, 119, 10863.

e) Bumm, L.A. ; Arnold, J.J. ; Cygan, M.T. ; Dunbar, T.D. ; Burgin, T.P. ; Jones, L. ; Allara, D.L. ; Tour, J.M. ; Weiss, P.S. *Science* **1996**,271,1705.

4) Martin, A.S. ; Sambles, J.R. Physical Review Letters 1993, 70, 218-221.) (Waldeck, D.H. ; Beratan, D.N. *Science* **1993**, 261, 576.

5)

a) Vogtle, F. ; Frank, M. ; Nieger, M. ; Belser, P. ; Zelewsky, A.V. ; Balzani, N. ; Barigelletti, F. ; Cola, L.D. ; Flamigni, L. *Angew. Chem. Int. Ed. Engl.* **1993**, 32, 1643.

b) Vollmer, M.S. ; Effenberger, F. ; Stumpig, T. ; Hartschuh, A. ; Port, H. ; Wolf, H. C. *J. Org. Chem*. **1998**, 63, 5080.

c) Zimmerman, H.E. ; Goldman, T.D. ; Hirzel, T.K. ; Schmidt, S.P. *J. Org. Chem*. **1980**, 45, 3933.

d) Tung, C.H. ; Zhang, L.P. ; Li, Y. ; Cao, H. ; Tanimoto, Y. *J. Am. Chem. Soc.* **1997**, 119, 5348.

e) Cao, H. ; Akimoto, Y. ; Fujiwara, Y. ; Tanimoto, Y. ; Zhang, L.P. ; Tung, C.H. *Bull. Chem. Soc. Jpn.* **1995**, 68, 3411.

f) Tung, C.H. ; Zhang, L.P. ; Li, Y. ; Cao, H. ; Tanimoto, Y. *J. Phys. Chem*. **1996**,100, 4480.

g) Splan, K.E. ; Keefe, M.H. ; Massari, A.M. ; Walters, K.A. ; Hupp, J.T. *Inorg. Chem*. **2002**, 41, 619.

h) Tan, Z. ; Kote, R. ; Samaniego, W.N. ; Weininger, S.J. ; McGimpsey, W.G. *J. Phys. Chem*. A **1999**, 103, 7612.

i) Bahr, J.L. ; Kodis, G. ; Garza, L. ; Lin, S. ; Moore, A.L. ; Moore, T.A. ; Gust, D. *J. Am. Chem. Soc.* **2001**, 123, 7124.

j) Oosterbaan, W.D. ; Koeberg, M. ; Piris, J. ; Havenith, R.W.A. ; Walree, C.A. ; Wegewijs, B.R. ; Jenneskens, L.W. ; Verhoeven, J.W. *J. Phys. Chem*. A **2001**,105, 5984.

k) Kumaresan, D. ; Agarwal, N. ; Ravikanth, M. *J. Chem. Soc., Perkin Trans.* 1, **2001**, 1644.

l) Kodis, G. ; Liddell, P.A. ; Garza, L. ; Clausen, C. ; Lindsey, J.S. ; Moore, A.L. ; Moore, T.A. ; Gust, D. *J. Phys. Chem*. A **2002**, 106, 2036.

m) Holten, D. ; Bocian, D.F. ; Lindsey, J.S. *Acc. Chem. Res*. **2002**, 35, 57.

n) Gonzales-Rodriguez, D. ; Torres, T. ; Guldi, D.M. ; Rivera, J. ; Echegoyen, L. *Organic Letters* **2002**, 4, 335.

o) Kimura, M. ; Hamakawa, T. ; Hanasuba, K. ; Shirai, H. ; Kobayashi, N. *Inorg. Chem*. **2001**, 40, 4775.

p) Prathapan, S. ; Yang, S.I. ; Seth, J. ; Miller, M.A. ; Bocian, D.F. ; Holten, D. ; Lindsey, J.S. *J. Phys. Chem. B* **2001**, 105, 8237.

q) Yang, S.I. ; Prathapan, S. ; Miller, M.A. ; Seth, J. ; Bocian, D.F. ; Lindsey, J.S. ; Holten, D. ; *J. Phys. Chem. B* **2001**, 105, 8249.

6)

a) Katayama, H. ; Ho, S. ; Yamamoto, M. *J. Phys. Chem.* **1992**, 96, 10115.

b) Bravo, J. ; Mendicuti, F. ; Mattice, W. *Macromol. Chem. Phys.* **1994**, 195, 3411.

c) Kaschke, M. ; Ernsting, N.P. ; Valeur, B. ; Bourson, J. *J. Phys. Chem.* **1990**, 94, 5757.

d) Hisada, K. ; Tsuchida, A. ; Ho, S. ; Yamamoto, M. *J. Phys. Chem. B* **1998**, 102, 2640.

e) Castellan, A. ; Kessab, L. ; Grelier, S. ; Nourmamode, A. ; Cotrait, M. ; Marsou, P. J. Phys. Chem. Soc. Perkin Trans. 2 1993,

f) Tran, J. ; Olmsted, J. *J. Photochem. Photobiol. A: Chem.* **1993**, 71, 45.

g) Lokowicz, J.R. ; Kusba, J. ; Gryczynski, I. ; Wiczk, W. ; Szmachinski, H. ; Johnson, M. *J. Phys. Chem.* **1991**, 95, 9654.

h) (Wagner, P.J. ; Klan, P. ; *J. Am. Chem. Soc.* **1998**, 120, 2198.

i) McGimpsey, W.G. ; Samaniego, W.N. ; Chen, L. ; Wang, F. *J. Phys. Chem.* A **1998**, 102, 8679.

j) Casa, M.D. ; Fabrizzi,L. ; Licchelli, M. ; Poggi, A. ; Russo, A. ; Taglietti, A. *Chem. Commun*. **2001**, 9, 825.

k) Apperloo, J.J. ; Martineau, C. ; Hal, P.A. ; Roncalli, J. ; Janssen, R.A.J. J. *Phys. Chem. A* **2002**,106, 21.

7) Levy, S.T. ; Shammai, S. *J. Chem. Phys*. **1992**, 96, 3585.

8)

a) Lokowicz, J.R. ; Kusba, J. ; Gryczynski, I. ; Wiczk, W. ; Szmachinski, H. ; Johnson, M. *J. Phys. Chem*. **1991**, 95, 9654.

b) Vollmer, M.S. ; Effenberger, F. ; Stumpig, T. ; Hartschuh, A. ; Port, H. ; Wolf, H. C. *J. Org. Chem*. **1998**, 63, 5080.

9) Inai, Y. ; Sisido, M. ; Imanishi, Y*. J. Phys. Chem*. **1991**,95, 3847.

10)

a)Batchelder, T.L. ; Fox, R.J. ; Meier, M.S. ; Fox, M.A. *J. Org. Chem.* **1996**, 61, 4206.

b) Galoppini, E. ; Fox, M.A. *J. Am. Chem. Soc*. 1996, 118, 2299.

c) Meier, M.S. ; Fox, M.A. ; Miller, J.R. *J. Org. Chem*. **1991**, 56, 5380.

d) Meier, M.S. ; Fox, M.A. ; Miller, J.R. *J. Org. Chem*. **1991**, 56, 5380.

11) McGimpsey, W.G. ; Chen, L. ; Carraway, R. ; Samaniego, W.N. *J. Phys. Chem. A* **1999**, 103, 6082.

12) Ghadiri, M.R. Granja, M.R. ; Milligan, R.A. ; McRee, D.E. ; Khazanovich, N. *Nature* **1993**, 366, 324.

13) .

a) Clark, T.D. ; Buriak, J.M. ; Kobayashi, K. ; Isler, M.P. ; McRee, D. E. ; Ghadiri, M.R. J*. Am. Chem. Soc*. **1998**,120, 8949.

b) Buriak, J.M. ; Ghadiri, M.R. *Material Science and Engineering* **1997**, C7, 207.

c) Granja, J.R. ; Ghadiri, M.R. *J. Am. Chem. Soc*. **1994**, 116, 10785.

d) Hartgerink, J.D. ; Granja, J.R. ; Milligan, R.A. ; Ghadiri, M.R. *J. Am. Chem. Soc*. **1996**, 118, 43.

e) Clark, T.D. ; Buehler, L.K. ; Ghadiri, M.R. J*. Am. Chem. Soc.* **1998**,120, 651.

f) Bong, D.T. ; Clark, T.D. ; Granja, J.R. ; Ghadiri, M.R. *Angew. Chem. Int. Ed.* **2001**, 40, 988.

14) Clark, T.D. ; Buriak, J.M. ; Kobayashi, K. ; Isler, M.P. ; McRee, D. E. ; Ghadiri, M.R. *J. Am. Chem. Soc*. **1998**,120, 8949.

15) Smith,G. A. ; McGimpsey, W.G. *J. Phys. Chem* **1994**, 98, 2923.

16) Murov, S.L. Handbook of Photochemistry; Marcel Dekker: New York, 1973.

17) Turro, N.J. Modern Molecular Photochemistry; University Science Books: Sausalito, CA, 1991.

18) Merrifield, R. B. *J. Am. Chem. Soc.* **1963**, 85, 2149.

19) Merrifield, R. B. *Biochemistry* **1964**, 3, 1385.

20) Carpino, L. A.; Han, G. Y. *J. Org. Chem.* **1972**, 37, 3404.

21)

a) Sen,A. ; Krishna, V. *Chem. Phys. Lett.* **1998**, 294, 499.

b) Mataga, N. ; Yao, H. ; Okada, T. ; Kanda. Y. ; Harriman, A. *Chem. Phys*. **1989**, 131, 473.